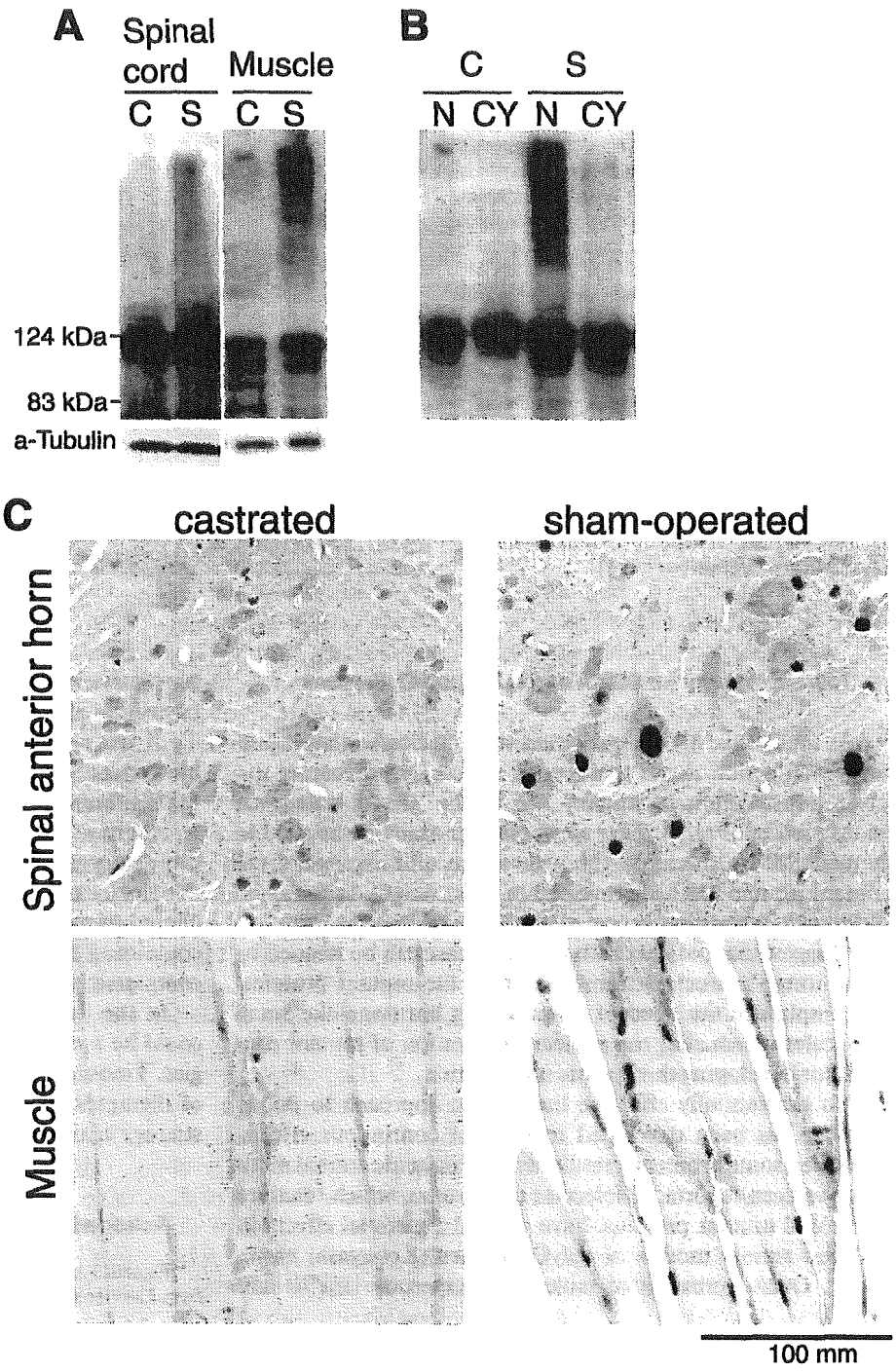

Fig. 4. Effects of castration on transgene expression and neuropathology of male AR-97Q mice. (**A**) Western blot analysis of total homogenates from the spinal cord and muscle of castrated (C) and sham-operated (S) male AR-97Q mice, that were immunolabeled by N-20. (**B**) Western blot analysis of nuclear (N) and cytoplasmic (CY) fraction from muscle of castrated (C) and sham-operated (S) male AR-97Q mice, immunolabeled by N-20. (**C**) Immunohistochemical study using 1C2 showed marked differences of diffuse nuclear staining and nuclear inclusions between castrated and sham-operated AR-97Q mice in the spinal anterior horn and muscle.

sir et al., 1995). More recently, conditional inactivation of wild-type huntingtin selectively in forebrain and testis resulted in a progressive degenerative neuronal phenotype and sterility (Dragatsis et al., 2000). Additionally, an anti-apoptotic effect of wild-type huntingtin was revealed in a cell model (Rigamonti et al., 2000). These results imply that loss of normal huntingtin function may contribute to the neurodegeneration in HD.

Androgens have been found to have neuroprotective effects. Administration of testosterone immediately after nerve injury impacts positively on functional recovery through actions mediated by the androgen receptor (Jones at al., 2001). In a cell culture model, AR with 24 CAGs showed trophic effects, whereas AR with 65 CAGs did not demonstrate any neuroprotection (Lieberman et al., 2002). The role of normal AR function in the pathogenesis of SBMA should be further studied in cell and animal models.

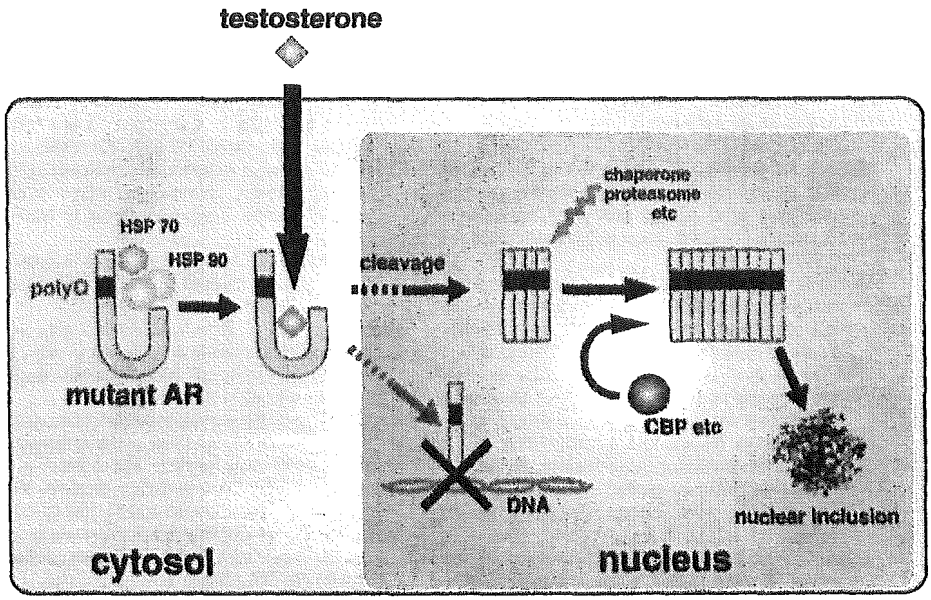

Fig. 5. Hypothetical dynamics of mutant AR in SBMA. In the absence of ligand, mutant AR is confined to a multi-heteromeric inactive complex with heat shock proteins (HSPs) and immunophilins in the cell cytoplasm. Upon testosterone-binding, the conformational change of mutant AR facilitates its dissociation from the complex and translocation into the nucleus. Mutant AR is cleaved and aggregates in the nucleus, whereas cellular mechanisms such as molecular chaperone and ubquitin-proteasome system attempt to mitigate its toxicity. Aggregation sequestrates critical cellular proteins such as CREB-binding protein (CBP) resulting in aberrant transcription, and finally forms nuclear inclusions. On the other hand, decreased transactivating function of mutant AR may contribute to the neurodegeneration and androgen insensitivity in SBMA.

Toward therapy for SBMA and other polyQ diseases

As mentioned above, our recent study indicated that testosterone reduction exerts therapeutic effects by preventing nuclear translocation of mutant AR in the SBMA transgenic mouse model (Fig. 5). This approach can easily be applied to human SBMA therapy. Although no specific ligand of the mutant protein has been revealed in other polyQ diseases, the striking therapeutic effects of castration in our SBMA mice further suggest that patients with polyQ disease can be rescued by preventing the nuclear translocation of the mutant proteins. We emphasize the need of investigating hormone-like small molecules which alter the nuclear localization of mutant proteins for developing therapeutic intervention.

No substantially effective therapeutic approach to polyQ diseases has been developed in spite of continuous efforts. However, some promising results using transgenic animal models have been reported. Molecular chaperones, which renature misfolded mutant proteins, have exerted beneficial effects in cell and animal models of polyQ diseases (Kobayashi et al., 2001). Over-expression of molecular chaperone HSP70 had preventive effects in cell and Tg mouse models of SBMA (Kobayashi et al., 2000; Adachi et al., 2003) as well as in an SCA1 Tg mouse model (Cummings et al., 2001). It may also be possible to treat SBMA by increasing the expression level or enhancing the function of molecular chaperones.

Alternatively, histone deacetylase inhibitors could be a promising candidate therapy for polyQ diseases (Steffan et al., 2001; Hockly et al., 2003). These drugs potentially correct altered transcription due to toxic effects of the mutant protein containing expanded polyQ, although their toxicity should be conquered before clinical application.

In the near future, an ideal treatment for polyQ diseases could be a combination of these and other therapeutic strategies. Transgenic mice will be useful in testing the effectiveness of therapies, and further contribute to the development of a strategy against polyQ diseases including SBMA.

Acknowledgements

Figures 3 and 4 are reprinted from Katsuno et al. (2002) with permission from Elsevier Science.

References

Abel A, et al: Expression of expanded repeat androgen receptor produces neurologic disease in transgenic mice. Hum molec Genet 10:107–116 (2001).

Adachi H, et al: Transgenic mice with an expanded CAG repeat controlled by the human AR promoter show polyglutamine nuclear inclusions and neuronal dysfunction without neuronal cell death. Hum molec Genet 10:1039–1048 (2001).

Adachi H, et al: HSP70 chaperone over-expression ameliorates phenotypes of the SBMA transgenic mouse model by reducing nuclear-localized mutant AR protein. J Neurosci 23:2203–2211 (2003).

Bingham PM, et al: Stability of an expanded trinucleotide repeat in the androgen receptor gene in transgenic mice. Nature Genet 9:191–196 (1995).

Brooks BP, et al: Characterization of an expanded glutamine repeat androgen receptor in a neuronal cell culture system. Neurobiol Dis 3:313–323 (1997).

Burright EN, et al: SCA1 transgenic mice: a model for neurodegeneration caused by an expanded CAG trinucleotide repeat. Cell 82:937–948 (1995).

Cummings CJ, et al: Over-expression of inducible HSP70 chaperone suppresses neuropathology and improves motor function in SCA1 mice. Hum molec Genet 10:1511–1518 (2001).

Danek A, et al: Decrease in androgen binding and effect of androgen treatment in a case of X-linked bulbospinal neuronopathy. Clin Investig 72:892–897 (1994).

DiFiglia M, et al: Aggregation of huntingtin in neuronal intranuclear inclusions and dystrophic neurites in brain. Science 277:1990–1993 (1997).

Doyu M, et al: Severity of X-linked recessive bulbospinal neuronopathy correlates with size of the tandem CAG repeat in androgen receptor gene. Ann Neurol 32:707–10 (1992).

Doyu M, et al: Androgen receptor mRNA with increased size of tandem CAG repeat is widely expressed in the neural and nonneural tissues of X-linked recessive bulbospinal neuronopathy. J Neurol Sci 127:43–47 (1994).

Dragatsis I, et al: Inactivation of Hdh in the brain and testis results in progressive neurodegeneration and sterility in mice. Nature Genet 26:300–306 (2000).

Goldenberg JN, et al: Testosterone therapy and the pathogenesis of Kennedy's disease (X-linked bulbospinal muscular atrophy). J Neurol Sci 135:158–161 (1996).
Gottlieb B, et al: Androgen insensitivity. Am J med Genet 89:210–217 (1999).
Hackam AS, Singaraja R, Zhang T, Gan L, Hayden MR: In vitro evidence for both the nucleus and cytoplasm as subcellular sites of pathogenesis in Huntington's disease. Hum molec Genet. 8:25–33 (1999).
Hockly E, et al: Suberoylanilide hydroxamic acid, a histone deacylase inhibitor, ameliorates motor deficits in a mouse model of Huntington's disease. Proc natl Acad Sci, USA 100:2041–2046 (2003).
Hodgson JG, et al: A YAC mouse model for Huntington's disease with full-length mutant huntingtin, cytoplasmic toxicity, and selective striatal neurodegeneration. Neuron 23:181–192 (1999).
Ikeda H, et al: Expanded polyglutamine in the Machado-Joseph disease protein induces cell death in vitro and in vivo. Nature Genet 13:196–202 (1996).
Jones KJ, et al: Neuroprotective effects of gonadal steroids on regenerating peripheral motoneurons. Brain Res Brain Res Rev 37:372–382 (2001).
Katsuno M, et al: Testosterone reduction prevents phenotypic expression in a transgenic mouse model of spinal and bulbar muscular atrophy. Neuron 35:843–854 (2002).
Katsuno M, et al: Leuprorelin rescues polyglutamine-dependent phenotypes in a transgenic mouse model of spinal and bulbar muscular atrophy. Nature Med 9:768–773 (2003).
Kennedy WR, et al: Progressive proximal spinal and bulbar muscular atrophy of late onset. A sex-linked recessive trait. Neurology 18:671–680 (1968).
Klement IA, et al: Ataxin-1 nuclear localization and aggregation: role in polyglutamine-induced disease in SCA1 transgenic mice. Cell 95:41–53 (1998).
Kobayashi Y, et al: Caspase-3 cleaves the expanded androgen receptor protein of spinal and bulbar muscular atrophy in a polyglutamine repeat length-dependent manner. Biochem biophys Res Commun 252:145–150 (1998).
Kobayashi Y, et al: Chaperones Hsp70 and Hsp40 suppress aggregate formation and apoptosis in cultured neuronal cells expressing truncated androgen receptor protein with expanded polyglutamine tract. J biol Chem 275:8772–8778 (2000).
Kobayashi Y, Sobue G: Protective effect of chaperones on polyglutamine diseases. Brain Res Bull 56:165–168 (2001).
La Spada AR, et al: Androgen receptor gene mutations in X-linked spinal and bulbar muscular atrophy. Nature 352:77–79 (1991).
La Spada AR, et al: Meiotic stability and genotype-phenotype correlation of the trinucleotide repeat in X-linked spinal and bulbar muscular atrophy. Nature Genet 2:301–304 (1992).
La Spada AR, et al: Androgen receptor YAC transgenic mice carrying CAG 45 alleles show trinucleotide repeat instability. Hum molec Genet 7:959–967 (1998).
Li M, et al: Nuclear inclusions of the androgen receptor protein in spinal and bulbar muscular atrophy. Ann Neurol 44:249–254 (1998).
Li M, et al: Nonneural nuclear inclusions of androgen receptor protein in spinal and bulbar muscular atrophy. Am J Pathol 153:695–701 (1998).
Lieberman AP, et al: Altered transcriptional regulation in cells expressing the expanded polyglutamine androgen receptor. Hum molec Genet 11:1967–1976 (2002).
MacLean HE, et al: Defects of androgen receptor function: from sex reversal to motor neuron disease. Mol Cell Endocr 112:133–141 (1995).
Mangiarini L, et al: Exon 1 of the HD gene with an expanded CAG repeat is sufficient to cause a progressive neurological phenotype in transgenic mice. Cell 87:493–506 (1996).
Mariotti C, et al: Phenotypic manifestations associated with CAG-repeat expansion in the androgen receptor gene in male patients and heterozygous females: a clinical and molecular study of 30 families. Neuromuscul Disord 10:391–397 (2000).
McCampbell A, et al: CREB-binding protein sequestration by expanded polyglutamine. Hum molec Genet 9:2197–2202 (2000).
McManamny P, et al: A mouse model of spinal and bulbar muscular atrophy. Hum molec Genet 11:2103–2111 (2002).
Merry DE, et al: Toward a mouse model for spinal and bulbar muscular atrophy: effect of neuronal expression of androgen receptor in transgenic mice. (abstract) Am J hum Genet 59 (suppl):A271 (1996).
Merry DE, et al: Cleavage, aggregation and toxicity of the expanded androgen receptor in spinal and bulbar muscular atrophy. Hum molec Genet 7:693–701 (1998).
Merry DE: Molecular pathogenesis of spinal and bulbar muscular atrophy. Brain Res Bull 56:203–207 (2001).
Mhatre AN, et al: Reduced transcriptional regulatory competence of the androgen receptor in X-linked spinal and bulbar muscular atrophy. Nature Genet 5:184–188 (1993).
Nasir J, et al: Targeted disruption of the Huntington's disease gene results in embryonic lethality and behavioral and morphological changes in heterozygotes. Cell 81:811–823 (1995).
Neuschmid-Kaspar F, et al: CAG-repeat expansion in androgen receptor in Kennedy's disease is not a loss of function mutation. Mol Cell Endocrinol 117:149–156 (1996).
Nucifora FC Jr, et al: Interference by huntingtin and atrophin-1 with CBP-mediated transcription leading to cellular toxicity. Science 291:2423–2428 (2001).
Peters MF, et al: Nuclear targeting of mutant Huntingtin increases toxicity. Mol Cell Neurosci 14:121–128 (1999).
Reddy PH, et al: Behavioural abnormalities and selective neuronal loss in HD transgenic mice expressing mutated full-length HD cDNA. Nature Genet. 20:198–202 (1998).
Rigamonti D, et al: Wild-type huntingtin protects from apoptosis upstream of caspase-3. J Neurosci 20:3705–3713 (2000).
Ross CA: Polyglutamine pathogenesis: emergence of unifying mechanisms for Huntington's disease and related disorders. Neuron 35:819–822 (2002).
Rubinsztein DC: Lessons from animal models of Huntington's disease. Trends Genet 18:202–209 (2002).
Saudou F, et al: Huntingtin acts in the nucleus to induce apoptosis but death does not correlate with the formation of intranuclear inclusions. Cell 95:55–66 (1998).
Schmidt BJ, et al: Expression of X-linked bulbospinal muscular atrophy (Kennedy disease) in two homozygous women. Neurology 59:770–772 (2002).
Sengelaub DR, et al: Hormonal control of neuron number in sexually dimorphic spinal nuclei of the rat: II. Development of the spinal nucleus of the bulbocavernosus in androgen-insensitive (Tfm) rats. J Comp Neurol 280:630–636 (1989).
Simeoni S, et al: Motoneuronal cell death is not correlated with aggregate formation of androgen receptors containing an elongated polyglutamine tract. Hum molec Genet 9:133–144 (2000).
Sobue G, et al: X-linked recessive bulbospinal neuronopathy. A clinicopathological study. Brain 112:209–232 (1989).
Sobue G, et al: Subclinical phenotypic expressions in heterozygous females of X-linked recessive bulbospinal neuronopathy. J Neurol Sci 117:74–78 (1993).
Steffan JS, et al: The Huntington's disease protein interacts with p53 and CREB-binding protein and represses transcription. Proc natl Acad Sci, USA 97:6763–6768 (2000).
Steffan JS, et al: Histone deacetylase inhibitors arrest polyglutamine-dependent neurodegeneration in Drosophila. Nature 413:739–743 (2001).
Stenoien DL, et al: Polyglutamine-expanded androgen receptors form aggregates that sequester heat shock proteins, proteasome components and SRC-1, and are suppressed by the HDJ-2 chaperone. Hum molec Genet 8:731–741 (1999).
Takeyama K, et al: Androgen-dependent neurodegeneration by polyglutamine-expanded human androgen receptor in *Drosophila*. Neuron 35:855–864 (2002).
Tanaka F, et al: Founder effect in spinal and bulbar muscular atrophy (SBMA). Hum molec Genet 5:1253–1257 (1996).
Tanaka F, et al: Tissue-specific somatic mosaicism in spinal and bulbar muscular atrophy is dependent on CAG-repeat length and androgen receptor-gene expression level. Am J hum Genet 65:966–973 (1999).
Tobin AJ, Signer ER: Huntington's disease: the challenge for cell biologists. Trends Cell Biol. 10:531–536 (2000).
Zhou ZX, et al: The androgen receptor: an overview. Recent Prog Horm Res 49:249–274 (1994).
Zhou ZX, et al: Specificity of ligand- dependent androgen receptor stabilization: receptor domain interactions influence ligand dissociation and receptor stability. Mol Endocrinol 9:208–218 (1995).
Zoghbi HY, Orr HT: Glutamine repeats and neurodegeneration. A Rev Neurosci 23:217–247 (2000).

Reprinted from JOURNAL OF NEUROLOGY, NEUROSURGERY & PSYCHIATRY, September 2003, Vol 74, No 9, p 1320-1322

SHORT REPORT

Sjögren's syndrome associated painful sensory neuropathy without sensory ataxia

K Mori, M Iijima, M Sugiura, H Koike, N Hattori, H Ito, M Hirayama, G Sobue

J Neurol Neurosurg Psychiatry 2003;**74**:1320–1322

Sensory neuropathy with prominent ataxia reflecting kinesthetic sensory impairment is a well recognised form of neuropathy associated with Sjögren's syndrome.[1–4] Pathologically, T cell invasion of dorsal root ganglia, loss of large sensory neurons, and secondary large fibre degeneration is seen in this neuropathy.[4] However, a form of neuropathy associated with Sjögren's syndrome, presenting with pain and superficial sensory involvement without sensory ataxia has been described anecdotally[5] and in a case report.[6] Clinicopathological details of the second form of neuropathy have not been elucidated. In this report we describe seven patients with Sjögren's syndrome showing painful sensory neuropathy without sensory ataxia.

Patients studied were referred for painful neuropathy to Nagoya University Hospital and its affiliated institutions. All seven patients fulfilled diagnostic criteria for Sjögren's syndrome by the American-European Consensus Group[7] and showed painful peripheral neuropathy (table 1). Patients included six women and one man, ranging from 25 to 72 years old. In all patients initial symptom of neuropathy was paraesthesia or painful dysaesthesia in the most distal portions of the extremities, later extending proximally to involve the entire legs and arms. The trunk became involved in three patients, and the trigeminal nerve was impaired in three patients. Asymmetry in sensory impairment was present in four patients. None of the patients showed sensory ataxia in the initial phase. Most patients retained essentially normal muscle strength, but patient 1 showed slight weakness in distal limb muscles. Painful sensation was the most characteristic, and this symptom compromised activities of daily living in all patients. Superficial sensation for pinprick and temperature was prominently impaired. Deep sensation such as joint position and vibratory sense was substantially well preserved. Sensory ataxia and Romberg's sign was not seen. Autonomic dysfunction was seen in four patients including Adie's pupils, urinary disturbance, and loss of ^{123}I-MIBG cardiac accumulation; however, orthostatic hypotension was not present. Apparent hypohidrosis was seen in three patients. Thermal stimulation in two patients, resulted in absent sweating on the forehead, trunk, arms, and legs, with preserved sweat gland function on pirocarpine test. Thermography showed abnormal skin temperature gradient in four patients. Deep tendon reflexes were comparatively well preserved except in two patients. Motor nerve conduction studies showed no slowing (mean (SD) 52.3 (3.9) m/s in the median, 44.8 (6.1) m/s in the tibial nerves) and preserved compound muscle action potentials (CMAPs) (7.5 (3.5) mV in the median, 9.0 (6.3) mV in the tibial nerves). Sensory nerve conduction (50.1 (6.0) m/s in the median, 47.2 (10.4) m/s in the sural nerves) and sensory nerve action potentials (SNAPs) (13.6 (11.7) uV in the median and 9.0 (6.3) uV in the sural nerves) were generally well preserved; only in patient 4, SNAPs were not evoked. Somatosensory evoked potentials (SEPs) were also well preserved (mean (SD) 20.0 (1.1) ms at N20, 13.7 (1.2) ms at N13, and 9.3 (0.4) ms at N9).

Sural nerve biopsy in five patients showed a variable degree of myelinated fibre loss, predominantly affecting small diameter fibres (table 1, fig 1). Unmyelinated fibre density also was severely reduced. Axonal sprouting was essentially absent in all patients. In teased fibre preparations, degeneration was seen in 32% to 55% of axons, predominantly small diameter fibres. Vasculitis was not seen.

Patient 2 developed sensory ataxia in the legs over the next nine years, and more details of this patient are given below. Patient 4 developed localised sensory ataxia in the fingers of the right hand over 11 years. Other patients showed persistent painful sensory neuropathy with gradual extension of distribution over 4 to 11 years of follow up.

CASE REPORT

A 68 year old man had painful dysaesthesia and numbness in the feet for about 10 years, with spread to the proximal of the legs and arms. When he was 56 years old, he noticed painful dysaesthesia in the legs, and subsequently in the hands. Neurological examination demonstrated light touch and pinprick were disturbed, and painful dysaesthesia was elicited in glove and stocking distribution. Vibration and joint position sense was comparatively well preserved for the first time. Sensory ataxia and Romberg's sign were not seen. Deep tendon reflexes were well preserved in upper limbs, but mildly decreased in lower limbs. Muscle strength was normal. Autonomic disturbance was not present. Nerve conductions were nearly normal except for sensory conduction in the median nerve, 40 m/s. SNAPs were well preserved. Result of routine blood haematology and biochemistry screening tests were normal. CSF protein was 33 mg/dl with no cells. A sural nerve biopsy specimen revealed myelinated fibre loss predominantly involving small diameter fibres with axonal degeneration.

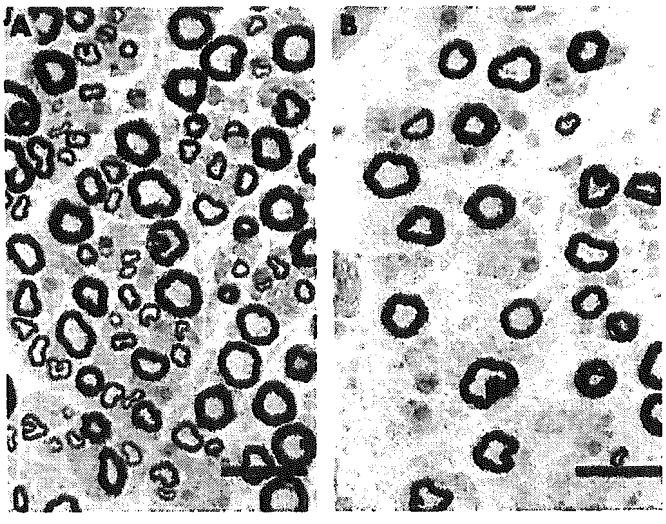

Figure 1 (A) Transverse section of a sural nerve specimen from a control subject. (B) Specimen from a patient of painful sensory neuropathy with predominant small fibre loss associated with Sjögren's syndrome (patient 1). Small diameter myelinated fibres are more noticeably involved and no axonal sprouting. Bars=25 μm.

Table 1 Clinical symptoms and histopathological findings

Patient Age/sex	Sjögren's syndrome, positive test	Neurological symptoms: Motor involvement Muscle atrophy/ strength	Sensory involvement: Distribution	Painful sensation	Nociception	Vibration/ position sense	Sensory ataxia	Romberg's sign	Autonomic signs	Sural nerve biopsy: Myelinated fibre density large, & small (no/mm²), Small/large ratio	Unmyelinated fibre density (no/mm²)	Follow up (y)
1 72/F	SS-A SS-B Sialography	+1 / +1	TL	+3	−3	−1 /−	−	−	1, 2, 4	axonal degeneration 1159, 921, 0.79	3463	6
2 68/M	SS-A Lip biopsy RB	−/−	L	+2	−3	−1 / −1	−*	−*	4	axonal degeneration 922, 448, 0.49 79, 169, 2.14‡	ND	2
3 36/F	Lip biopsy RB	−/−	TL	+3	−3	−/−	−	−	3	axonal degeneration 1876, 1332, 0.71	2585	6
4 71/F	SS-A Sialography RB	+1 /−	L	+3	−3	−2 / −2	−†	−	1, 2, 4	axonal degeneration 1158, 1553, 1.34	8312	11
5 48/F	Lip biopsy Gum test	−/−	FL	+3	−3	−/−	−	−	−	axonal degeneration 2541, 1528, 0.62	3232	11
6 25/F	SS-A RB	−/−	FL	+3	−3	−/−	−	−	1	ND	ND	6
7 62/F	Lip biopsy Schirmer's test	−/−	FL	+3	−3	−/−	−	−	−	ND	ND	4
Controls (mean (SD), n=9)									3068 (294),	5122 (438), 1.7 (0.2)	29913 (3457)	

+, Positive findings; −, negative findings. Muscle weakness, atrophy, and painful sensation: +3, severe; +2, moderate; +1, mild; −, absent. Distribution of sensory involvement: F, facial; T, trunk; L, limbs. Sensory signs: −3, severe; −2, moderate; −1, mild; −, absent. Nociception was evaluated by pin pricking. Autonomic dysfunction: 1, Adie's pupils; 2, loss of ^{123}I-MIBG cardiac accumulation; 3, urinary disturbance; 4, hypohidrosis. SS-A, anti-SS-A antibody; SS-B, anti-SS-B antibody; RB, Rose Bengal test for Sjögren's syndrome. For nerve biopsy findings, large >6.73 um; small <6.73 µm in fibre diameter; As for typical sensory ataxic neuropathy with Sjögren's syndrome, large myelinated fibre density was 660 (714) [mean (SD)], small myelinated fibre density was 3263 (2390), and small/large fibre ratio was 14.6 (19.0) for 20 cases. ND, not determined. *,†Sensory ataxia developed in the legs 9 years later, in the right hand 11 years later respectively. ‡Result of second sural nerve biopsy examined 12 years later.

In the next nine years, involvement of deep sensation gradually developed. At 68 years old, he showed sensory ataxia in the legs and positive Romberg's sign without muscle weakness. The deep tendon reflexes were almost absent. Motor nerve conduction velocities were still preserved, but sensory nerve action potentials were not elicited in the median and sural nerves. At this time, sicca symptoms were obvious, and a Rose Bengal test was positive. A lip biopsy specimen showed periacinar lymphocytic infiltration. Second sural nerve biopsy on the other side showed severe large fibre loss as well as small fibre loss without axonal sprouts.

DISCUSSION

The most well recognised form of Sjögren's syndrome associated neuropathy has been sensory ataxic neuropathy associated with profound impairment of kinesthetic sensation.[1–4 8–10] Neuropathologically, T cell invasion in the dorsal root ganglion as well as loss of large ganglion neurons and their large axons have been verified.[4] However clinicopathological findings in our patients differed remarkably from those of sensory ataxic neuropathy. Painful sensation and hyperalgia in our patients suggested involvement of small nociceptive nerve fibres as has been demonstrated.[11]

Indeed, in sural nerve of our patients, small myelinated and unmyelinated fibres were predominantly involved; electrophysiologically, amplitudes of SNAPs were comparatively preserved, particularly in contrast with sensory ataxic neuropathy. Findings in the dorsal root ganglion in this neuropathy have not been described, but predominant small fibre loss, extremely rare axonal sprouts, lack of vasculitis, lack of motor involvement, and fairly well preserved SEPs suggest that small dorsal root ganglion neurons can be involved.

As demonstrated by the clinical course of our patients, some patients show persistent symptoms or a slowly progressive course while remaining limited to a painful small fibre type of neuropathy, while others, including one of our patients, may later develop sensory ataxic neuropathy presumably involving large sensory neurons. Additionally, one of our patients developed localised unilateral sensory ataxia in the fingers, suggesting that some patients may develop localised sensory ataxia. These observations suggest that painful sensory neuropathy with predominant small fibre loss and sensory ataxic large fibre neuropathy are elements of a spectrum of sensory neuropathy in Sjögren's syndrome.

In summary, these patients suggest that painful sensory neuropathy with predominant small fibre loss is an identifiable subtype of Sjögren's syndrome associated neuropathy.

Authors' affiliations
K Mori, M Iijima, M Sugiura, H Koike, N Hattori, H Ito, M Hirayama, G Sobue, Department of Neurology, Nagoya University Graduate School of Medicine, Nagoya, Japan

Competing interests: none declared.

Correspondence to: Dr G Sobue, Department of Neurology, Nagoya University Graduate School of Medicine, Nagoya 466–8550 Japan; sobueg@med.nagoya-u.ac.jp

Received 31 October 2002
In revised form 26 January 2003
Accepted 14 March 2003

REFERENCES

1 **Kennett RP**, Harding AE. Peripheral neuropathy associated with the sicca syndrome. *J Neurol Neurosurg Psychiatry* 1986;**49**:90–2
2 **Graus F**, Pou A, Kanterewicz E, *et al.* Sensory neuronopathy and Sjögren's syndrome: clinical and immunologic study of two patients. *Neurology* 1988;**38**:1637–9.
3 **Gemignani F**, Marbini A, Pavesi G, *et al.* Peripheral neuropathy associated with primary Sjögren's syndrome. *J Neurol Neurosurg Psychiatry* 1994;**57**:983–6.
4 **Griffin JW**, Cornblath DR, Alexander E, *et al.* Ataxic sensory neuropathy and dorsal root ganglionitis associated with Sjögren's syndrome. *Ann Neurol* 1990;**27**:304–15.
5 **Grant IA**, Hunder GG, Homburger HA, *et al.* Peripheral neuropathy associated with sicca complex. *Neurology* 1997;**48**:855–62.
6 **Denislic M**, Meh D, Popovic M, *et al.* Small nerve fibre dysfunction in a patient with Sjögren's syndrome. Neurophysiological and morphological confirmation. *Scand J Rheumatol* 1995;**24**:257–9.
7 **Vitali C**, Bombardieri S, Jonsson R, *et al.* Classification criteria for Sjögren's syndrome: a revised version of the European criteria proposed by the American-European Consensus Group. *Ann Rheum Dis* 2002;**61**:554–8.
8 **Sobue G**, Yasuda T, Kachi T, *et al.* Chronic progressive sensory ataxic neuropathy: clinicopathological features of idiopathic and Sjögren's syndrome-associated cases. *J Neurol* 1993;**240**:1–7.
9 **Kumazawa K**, Sobue G, Yamamoto K, *et al.* Segmental anhidrosis in the spinal dermatomes in Sjögren's syndrome-associated neuropathy. *Neurology* 1993;**43**:1820–3.
10 **Mori K**, Koike H, Misu K, *et al.* Spinal cord magnetic resonance imaging demonstrates sensory neuronal involvement and clinical severity in neuronopathy associated with Sjögren's syndrome. *J Neurol Neurosurg Psychiatry* 2001;**71**:488–92.
11 **Wokke JH**, van Dijk GW. Sensory neuropathies including painful and toxic neuropathies. *J Neurol* 1997;**244**:209–21.

The EMBO Journal (2004) 23, 1977–1986 | © 2004 European Molecular Biology Organization | All Rights Reserved 0261-4189/04
www.embojournal.org

THE EMBO JOURNAL

A novel protein-conjugating system for Ufm1, a ubiquitin-fold modifier

Masaaki Komatsu[1], Tomoki Chiba[1], Kanako Tatsumi[1], Shun-ichiro Iemura[2], Isei Tanida[3], Noriko Okazaki[4], Takashi Ueno[3], Eiki Kominami[3], Tohru Natsume[2] and Keiji Tanaka[1,*]

[1]Department of Molecular Oncology, Tokyo Metropolitan Institute of Medical Science, Bunkyo-ku, Tokyo, Japan, [2]National Institutes of Advanced Industrial Science and Technology, Biological Information Research Center (JBIRC), Kohtoh-ku, Tokyo, Japan, [3]Department of Biochemistry, Juntendo University School of Medicine, Bunkyo-ku, Tokyo, Japan and [4]Kazusa DNA Research Institute, Kazusa-Kamatari, Kisarazu, Chiba, Japan

Several studies have addressed the importance of various ubiquitin-like (UBL) post-translational modifiers. These UBLs are covalently linked to most, if not all, target protein(s) through an enzymatic cascade analogous to ubiquitylation, consisting of E1 (activating), E2 (conjugating), and E3 (ligating) enzymes. In this report, we describe the identification of a novel ubiquitin-fold modifier 1 (Ufm1) with a molecular mass of 9.1 kDa, displaying apparently similar tertiary structure, although lacking obvious sequence identity, to ubiquitin. Ufm1 is first cleaved at the C-terminus to expose its conserved Gly residue. This Gly residue is essential for its subsequent conjugating reactions. The C-terminally processed Ufm1 is activated by a novel E1-like enzyme, Uba5, by forming a high-energy thioester bond. Activated Ufm1 is then transferred to its cognate E2-like enzyme, Ufc1, in a similar thioester linkage. Ufm1 forms several complexes in HEK293 cells and mouse tissues, revealing that it conjugates to the target proteins. Ufm1, Uba5, and Ufc1 are all conserved in metazoa and plants but not in yeast, suggesting its potential roles in various multicellular organisms.
The EMBO Journal (2004) **23**, 1977–1986. doi:10.1038/sj.emboj.7600205; Published online 8 April 2004
Subject Categories: proteins
Keywords: Uba5; ubiquitin; ubiquitin fold; ubiquitin-like protein; Ufm1

Introduction

Protein modification plays a pivotal role in the regulation and expansion of genetic information. In the past two decades, a new type of post-translational protein-modifying system has been identified whose uniqueness is that protein(s) is used as a ligand, that is, modification of protein, by protein, and for protein. A typical system is the ubiquitylation, a modification system in which a single or multiple ubiquitin molecules are attached to a protein, which serves as a signaling player that controls a variety of cellular functions (Hershko and Ciechanover, 1998; Pickart, 2001). Protein ubiquitylation is catalyzed by an elaborate system highly regulated in the cells, which is catalyzed by a sequential reaction of multiple enzymes consisting of activating (E1), conjugating (E2), and ligating (E3) enzymes. E1, which initiates the reaction, forms a high-energy thiolester bond with ubiquitin via adenylation in an ATP-dependent manner. The E1-activated ubiquitin is then transferred to E2 in a thioester linkage. In some cases, E2 can directly transfer the ubiquitin to substrate proteins in an isopeptide linkage; however, E2s mostly requires the participation of E3 to achieve substrate-specific ubiquitylation reaction in the cells. E3s are defined as enzymes required for recognition of specific substrates for ubiquitylation, other than E1 and E2 (Varshavsky, 1997; Bonifacino and Weissman, 1998; Glickman and Ciechanover, 2002).

A set of novel molecules called ubiquitin-like proteins (UBLs) that have structural similarities to ubiquitin has been recently identified (Jentsch and Pyrowolakis, 2000). They are divided into two subclasses: type-1 UBLs, which ligate to target proteins in a manner similar, but not identical, to the ubiquitylation pathway, such as SUMO, NEDD8, and UCRP/ISG15, and type-2 UBLs (also called UDPs, ubiquitin-domain proteins), which contain ubiquitin-like structure embedded in a variety of different classes of large proteins with apparently distinct functions, such as Rad23, Elongin B, Scythe, Parkin, and HOIL-1 (Tanaka *et al*, 1998; Jentsch and Pyrowolakis, 2000; Yeh *et al*, 2000; Schwartz and Hochstrasser, 2003).

In this report, we describe a unique human UBL-type modifier named ubiquitin-fold modifier 1 (Ufm1) that is synthesized in a precursor form consisting of 85 amino-acid residues. We also identified the human activating (Uba5) and conjugating (Ufc1) enzymes for Ufm1. Prior to activation by Uba5, the extra two amino acids at the C-terminal region of the human proUfm1 protein are removed to expose Gly whose residue is necessary for conjugation to target molecule(s). Lastly, we show that the mature Ufm1 is conjugated to yet unidentified endogenous proteins, forming ~28, 38, 47, and 70 kDa complexes in human HEK293 cells and various mouse tissues.

Results

Identification of a novel protein-activating enzyme, Uba5

Our initial plan was to identify the molecule(s) that interacts with human Atg8p homolog GATE16, a type-1 UBL modifier required for autophagy (Klionsky and Emr, 2000; Ohsumi, 2001), using a yeast two-hybrid screening. Please note that the nomenclature of the autophagy-related genes was recently unified as *ATG* (Klionsky *et al*, 2003). Among several

*Corresponding author. Department of Molecular Oncology, The Tokyo Metropolitan Institute of Medical Science, 3-18-22 Honkomagome, Bunkyo-ku, Tokyo 113-8613, Japan. Tel.: +81 3 3823 2237; Fax: +81 3 3823 2237; E-mail: tanakak@rinshoken.or.jp

Received: 1 December 2003; accepted: 15 March 2004; published online: 8 April 2004

positive clones, we identified fragments of FLJ23251 (Figure 1A), which encodes a 404-amino-acid protein highly conserved in various multicellular organisms, such as *Homo sapiens*, *Caenorhabditis elegans*, *Drosophila melanogaster*, and *Arabidopsis thaliana*, but absent in yeasts (*Saccharomyces cerevisiae* and *Schizosaccharomyces pombe*) (Figure 1B). The sequence of FLJ23251 in the region containing residues 72–229 is highly homologous to the corresponding regions in Uba1 (i.e., E1 for ubiquitin) and other E1-like proteins for UBLs including the ATP-binding motif (G*X*G*XX*G) (Figure 1A and B). We named this protein Uba5, because it is a member of the E1-like enzyme family. Uba5 also has a metal-binding motif conserved in other E1-like enzymes such as Uba2, Uba3, Uba4, and Atg7. Most of E1-like enzymes have an active site Cys residue within the conserved 10–20 amino-acid residues downstream from the metal-binding

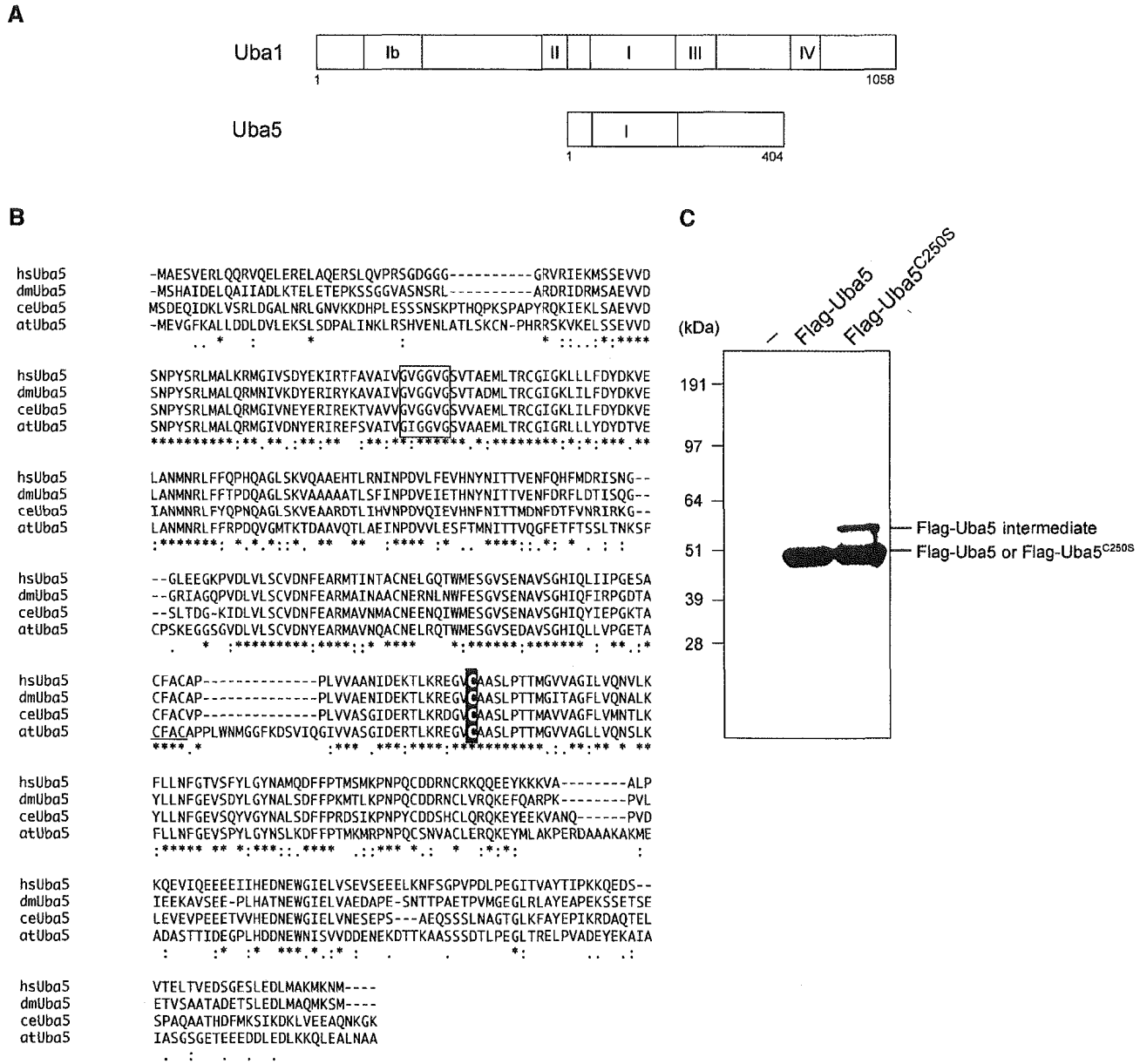

Figure 1 Uba5, a novel E1-like enzyme. (**A**) Schematic representation of Uba1 and Uba5 in *H. sapiens*. Uba1 is divided into several domains, including I, Ib, II, III, and IV boxes, which are conserved in other E1-like enzymes, and other regions without obvious similarity, described previously (Komatsu *et al*, 2001). Note that Uba5 is of a relatively small size and includes the box I and two other parts. The box I region of Uba1 (amino acids 459–611) has 48.4% similarity and 22.3% identity to amino acids 72–229 of Uba5, which includes the conserved ATP-binding motif (G*X*G*XX*G). The sequence of Uba5 is available from GenBank™ under the accession number AK026904. hs, *H. sapiens*; ce, *C. elegans*; dm, *D. melanogaster*; at, *A. thaliana*. (**B**) Sequence alignment of hsUba5 and its homologs of other species (dm, NM_132494; ce, NM_058847; at, NM_100414). The amino-acid sequence of hsUba5 is compared by the ClustalW program. *Asterisks*, identical amino acids; *single* and *double dots*, weakly and strongly similar amino acids, respectively, determined by the criteria of ClustalW program. *Open box* indicates an ATP-binding motif. The putative active site Cys residue is boxed in black. The metal-binding motif is underlined. (**C**) Identification of the intermediate linked to Uba5 in HEK293 cells. Both Uba5 and Uba5^{C250S}, in which the predicted active site Cys positioned at 250 was changed to Ser by site-directed mutagenesis, were tagged with Flag peptide at N-terminus, resulting in Flag-Uba5 and Flag-Uba5^{C250S}, respectively. Each Flag-Uba5 and Flag-Uba5^{C250S} was expressed in HEK293 cells. The cell lysates were subjected to SDS–PAGE and analyzed by immunoblotting with anti-Flag antibody.

motif. In the case of Uba5, the Cys^{250} seems to be the most possible active site Cys residue (Figure 1B). If an active site Cys residue within an E1 and E1-like enzymes is changed to Ser, an O-ester bond instead of a thioester bond is formed with its respective modifier protein and the intermediates become stable even under reducing conditions. Therefore, we mutated Cys^{250} within Uba5 to Ser and expressed it as a Flag-fused $Uba5^{C250S}$ (Flag-$Uba5^{C250S}$) or Flag-Uba5 as control in HEK293 cells. As shown in Figure 1C, both Flag-Uba5 and Flag-$Uba5^{C250S}$ were expressed as ~50 kDa proteins in HEK293 cells. When Flag-$Uba5^{C250S}$ was expressed, an additional band with a higher molecular mass of ~60 kDa was clearly observed, indicating that Flag-$Uba5^{C250S}$ forms an intermediate complex with an endogenous protein. These results suggest that Uba5 is indeed a novel protein-activating enzyme for a presumptive modifier (see below).

Identification of a novel ubiquitin-fold molecule, Ufm1

Because Uba5 was identified as GATE-16-binding protein, we initially assumed that Uba5 is another GATE-16-activating enzyme, in addition to Atg7. To test this possibility, we examined whether $Uba5^{C250S}$ (the presumptive active site Cys at position 250 was replaced by Ser) forms an intermediate complex with GATE-16 or not. Unexpectedly, we could not identify a stable complex between $Uba5^{C250S}$ and GATE-16 (data not shown). Therefore, we attempted to identify a protein(s) that physically associates with Uba5 in the cells. To do this, Flag-Uba5 was expressed in HEK293 cells, then immunoprecipitated by anti-Flag antibody. The immunoprecipitates were eluted with a Flag peptide, then digested with Lys-C endopeptides (*Achromobacter* protease I) and the cleaved fragments were directly analyzed using a highly sensitive 'direct nano-flow LC–MS/MS' system as described in Materials and methods. Following database search, a total of 28 peptides were assigned to MS/MS spectra obtained from four nano-LC–MS/MS analyses for the Flag-Uba5-associated complexes. These peptide data identified three proteins as Uba5-associated components: GATE-16, and hypothetical proteins BM-002 and CGI-126 (excluding the bait protein Uba5 and the background proteins, such as HSP70 and keratins).

One of these identified proteins, BM-002, is an 85-amino-acid protein with a predicted molecular mass of ~9.1 kDa. This protein is conserved in multicellular organisms, but not in yeasts, like Uba5 (Figure 2A). The human BM-002 has high identity over the species in the central region but has elongated sequences at both N- and C-terminal regions in some species. Although the protein shows no clear overall sequence identity to ubiquitin or other modifiers (Figure 2B), the tertiary structure of BM-002 displays a striking resemblance to human ubiquitin (Figure 2C). The human structure of BM-002 was constructed by a computer-assisted modeling, based on the structure of its *C. elegans* homolog that has been analyzed previously, as a protein possessing 'ubiquitin-like fold' with secondary structure elements ordered β–β–α–β–β–α (α-helix and β-sheet) along the sequence (Cort *et al*, 2002). Thus, we named human BM-002 as Ufm1.

Ubiquitin is synthesized in a precursor form that must be processed by de-ubiquitylating enzymes (DUBs) to generate a Gly–Gly sequence at the C-terminus. Similarly, Ufm1 has a single Gly residue conserved across species at the C-terminal region, although the length and sequences of amino acids extending from this Gly residue vary among species. To test whether the C-terminus of Ufm1 is post-translationally cleaved, we constructed an expression vector for Ufm1 tagged at both the N- and C-ends, that is, a Flag epitope at the N-terminus and an HA epitope at the C-terminus (Flag-Ufm1-HA) (Figure 2D). After transfection of Flag-Ufm1-HA into HEK293 cells, the cell lysate was subjected to SDS–PAGE, and Flag-Ufm1-HA was detected by immunoblotting. A 10-kDa protein corresponding to Ufm1 was recognized with anti-Flag antibody, while no appreciable protein was observed with anti-HA antibody (Figure 2E, lanes 2 and 7). The mobility on SDS–PAGE was similar to that of Flag-Ufm1ΔC2 (equivalent to mature $Ufm1^{1-83}$ protein) lacking the C-terminal Ser^{84} and Cys^{85} of proUfm1 (Figure 2E, lane 4). These results suggested that the C-terminus of Ufm1 is post-translationally cleaved in the cells, producing mature Ufm1 with the C-terminal Gly^{83} residue. It is known that the replacement of C-terminal Gly residue of Ub and other UBLs with an Ala residue inhibits the C-terminal processing (Kabeya *et al*, 2000; Tanida *et al*, 2003). To examine whether Gly^{83} of Ufm1 is essential for the cleavage, Gly^{83} of Flag-Ufm1-HA was mutated to Ala, and expressed in HEK293 cells (Figure 2D, Flag-$Ufm1^{G83A}$-HA). The mobility of most Flag-$Ufm1^{G83A}$-HA on SDS–PAGE was apparently slower than that of Flag-Ufm1-HA (Figure 2E, lane 3). This mutant was recognized by immunoblotting with anti-HA antibody as well as anti-Flag antibody, suggesting that mutation Gly^{83} to Ala confers resistance to its C-terminal cleavage.

Uba5 is an Ufm1-activating enzyme

We next investigated whether Uba5 forms an intermediate complex with Ufm1. We expressed Flag-Uba5 or Flag-$Uba5^{C250S}$ with Myc-tagged Ufm1 (Myc-Ufm1) in HEK293 cells. Myc-tagged Ufm1ΔC3 lacking the C-terminal Gly^{83} of mature Ufm1 (Myc-Ufm1ΔC3; i.e., deletion form of three residues from precursor $Ufm1^{1-85}$ protein) was used as control. Each cell lysate was prepared and analyzed by immunoblotting with anti-Flag antibody. Flag-$Uba5^{C250S}$ formed an intermediate with an endogenous protein as shown in Figure 1 (Figure 3A, lane 7). When Flag-$Uba5^{C250S}$ was coexpressed with Myc-Ufm1, the intermediate shifted to higher molecular weight (Figure 3A, lane 8). The higher band was not detected when Myc-Ufm1ΔC3 was coexpressed (Figure 3A, lane 9). To verify that the intermediate is indeed the Uba5–Ufm1 complex, Flag-$Uba5^{C250S}$ was immunoprecipitated and blotted with anti-Flag and anti-Myc antibody. Consistent with the above data, a higher sized intermediate was observed when Flag-$Uba5^{C250S}$ was coexpressed with Myc-Ufm1 (Figure 3B, top panel, lane 5), but not alone or with Myc-Ufm1ΔC3 (Figure 3B, top panel, lanes 4 and 6). The intermediate was also recognized by anti-Myc antibody (Figure 3B, lower panel, lane 5), indicating the existence of the Flag-$Uba5^{C250S}$–Myc-Ufm1 complex. Note that the small-sized intermediate is presumably a complex with an endogenous Ufm1, as mentioned. These results indicate that Uba5 forms an intermediate with Ufm1 and the Gly^{83} residue of Ufm1 is essential for the formation of the intermediate with Uba5 *in vivo*.

We subsequently tested whether Uba5 can activate Ufm1 *in vitro*. The thioester formation assay was performed using recombinant proteins expressed in *Escherichia coli*. Recombinant GST-tagged Uba5 and mature Ufm1

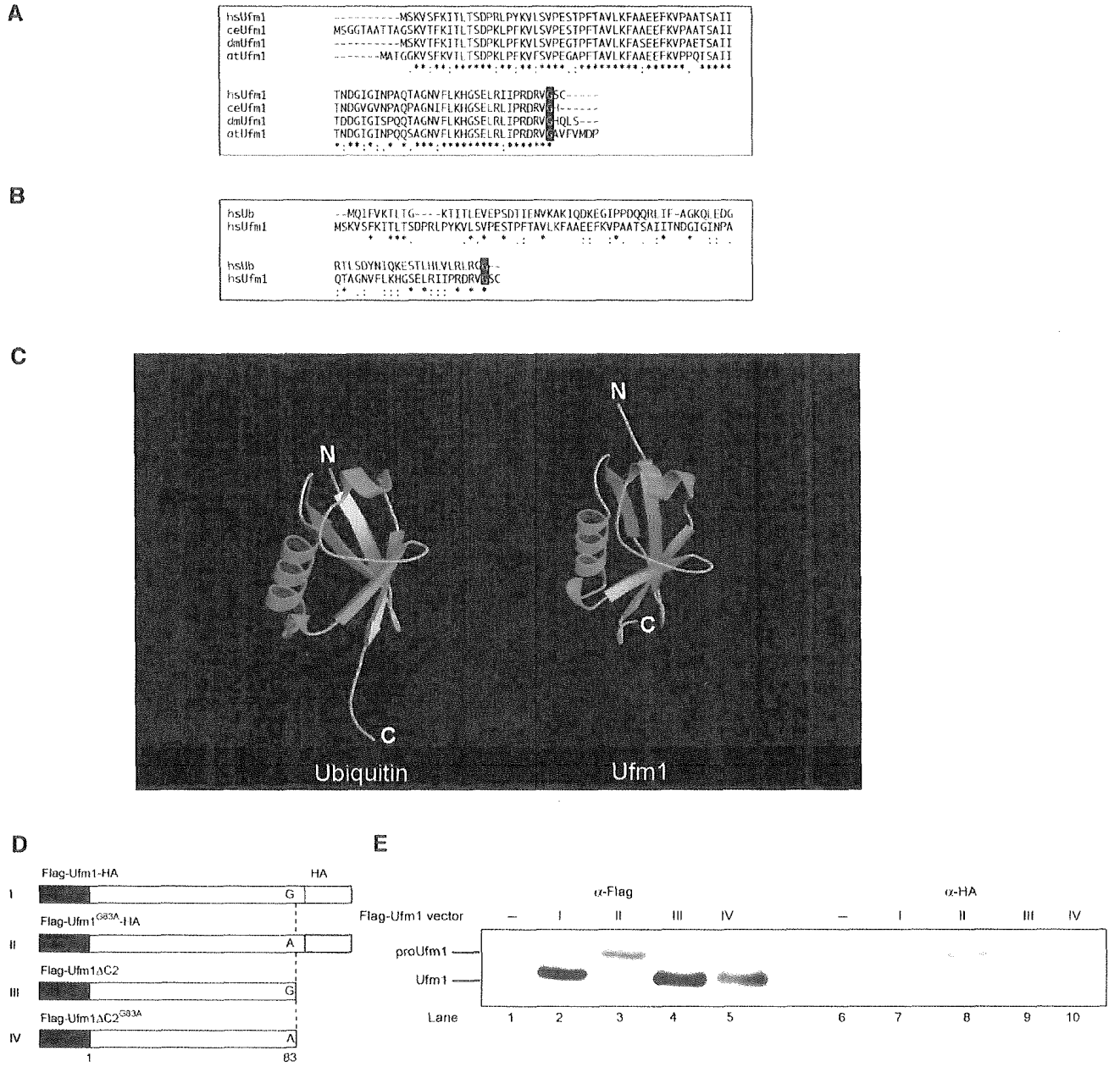

Figure 2 Ufm1, a novel ubiquitin-fold molecule. (**A**) Sequence alignment of hsUfm1 and its homologs. The sequence of hsUfm1 is available from GenBank™ under the accession number BC005193 (dm, a coding region of dmUfm1 was found from *D. melanogaster* genomic sequence; ce, NM_066304; at, NM_106420). The homology analysis was performed as described in Figure 1B. The C-terminal conserved Gly residue is boxed in black. (**B**) Sequence alignment of hsUbiquitin with hsUfm1. The homology analysis was performed as described in Figure 1B. The C-terminal conserved Gly residue is boxed in black. (**C**) Structural ribbon of hsUbiquitin and predicted structural ribbon of hsUfm1. α-Helices and β-strands are shown in green and yellow, respectively. The homology model of hsUfm1 was created from the *C. elegans* Ufm1 structure (Cort *et al*, 2002) by using MOE program (2003.02; Chemical Computing Group Inc., Montreal, Quebec, Canada). (**D**) Schematic representation of mammalian expression plasmids for Ufm1 and the derivative mutants. Flag epitope tags at the N-terminus, HA epitope tags at the C-terminus, and putative cleavage site Gly^{83} residue (vertical dotted lines) are indicated. To construct $Ufm1^{G83A}$, a single point mutation was introduced into Ufm1, which led to an amino-acid substitution from Gly to Ala at position 83. To construct Ufm1ΔC2, the two C-terminal residues were deleted by PCR. $Ufm1\Delta C2^{G83A}$ was also produced by site-directed mutagenesis of Ufm1ΔC2. The ΔC2 mutants were tagged with the Flag epitopes at N-terminus. (**E**) ProUfm1 processing. HEK293 cells were transfected with Flag-Ufm1-HA, Flag-$Ufm1^{G83A}$-HA, Flag-Ufm1ΔC2, or Flag-$Ufm1\Delta C2^{G83A}$. The cell lysates were subjected to SDS–PAGE and analyzed by immunoblots with anti-Flag and anti-HA antibodies. ProUfm1 and mature Ufm1 are indicated on the left. The numbers at the top from I to IV are similar to those in (D).

(Ufm1ΔC2) with exposed C-terminal Gly^{83} residue were purified, mixed and incubated in the presence of ATP and then subjected to SDS–PAGE at either reducing or nonreducing conditions. GST-Ufm1ΔC3 was used as control. An ~100 kDa band corresponding to the GST-Ufm1ΔC2–GST-Uba5 intermediate complex was clearly observed when the mixture was applied at nonreducing conditions (Figure 3C, lane 3). This intermediate was not observed when ATP or GST-Uba5 was excluded from the mixture (Figure 3C, lanes 1 and 2), or when the mixture was loaded in the presence of

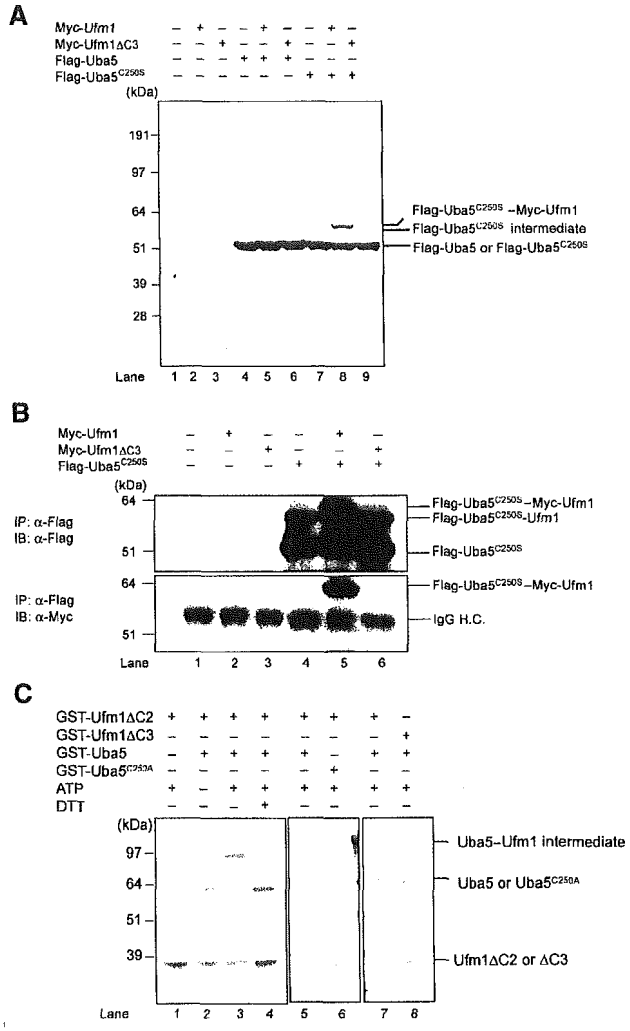

Figure 3 Demonstration that Uba5 is an Ufm1-activating enzyme. (**A**) Immunoblotting analysis. Each Myc-tagged Ufm1 (Myc-Ufm1) and Myc-Ufm1ΔC3 was expressed alone (lanes 2 and 3, respectively), and coexpressed with Flag-Uba5 (lanes 5 and 6, respectively) or Flag-Uba5^{C250S} (lanes 8 and 9, respectively). Each Flag-Uba5 and Flag-Uba5^{C250S} was also expressed alone (lanes 4 and 7, respectively). The cell lysates were subjected to SDS–PAGE and analyzed by immunoblotting with anti-Flag antibody. The bands corresponding to Flag-Uba5, Flag-Uba5^{C250S}, and Flag-Uba5^{C250S} intermediates are indicated on the right. (**B**) Immunoblotting analysis after immunoprecipitation. Each Myc-Ufm1 and Myc-Ufm1ΔC3 was expressed alone (lanes 2 and 3, respectively), and coexpressed with Flag-Uba5^{C250S} (lanes 5 and 6, respectively). Flag-Uba5^{C250S} was also expressed alone (lane 4). The cell lysates were immunoprecipitated with anti-Flag antibody. The resulting immunoprecipitates were subjected to SDS–PAGE and analyzed by immunoblotting with anti-Flag and anti-Myc antibodies. The bands corresponding to Flag-Uba5^{C250S}, Flag-Uba5^{C250S}–endogenous Ufm1, and Flag-Uba5^{C250S}–Myc-Ufm1 intermediates are indicated. (**C**) *In vitro* activating assay of Ufm1 by Uba5. Purified recombinant GST-Ufm1ΔC2 (2 μg) (lanes 1–7) was incubated for 30 min at 25°C with some of the following: 2 μg of purified recombinant GST-Uba5 (lanes 2–5, 7, and 8), GST-Uba5^{C250A} (lane 6), and 5 mM ATP (lanes 1 and 3–8). Lane 8 was conducted similar to lane 7, except that GST-Ufm1ΔC3 was used instead of GST-Ufm1ΔC2. Reactions were then incubated with SDS loading buffer lacking reducing agent (lanes 1–3 and 5–8) or containing 100 mM DTT (lane 4). The presence or absence of various components is indicated above the lanes. The bands corresponding to free GST-Uba5, GST-Uba5^{C250A}, GST-Ufm1ΔC2 (mature Ufm1), GST-Ufm1ΔC3, and GST-Uba5–GST-Ufm1ΔC2 thioester product are indicated on the right.

a reducing agent dithiothreitol (DTT) (Figure 3C, lane 4). Furthermore, GST-tagged Uba5^{C250A} mutant, a presumptive active site Cys mutant, could not form the intermediate even at nonreducing conditions (Figure 3C, lane 6). GST-tagged Ufm1ΔC3 was also incapable of forming the intermediate in this reaction (Figure 3C, lane 8). Taken together, we concluded that Uba5 is an Ufm1-activating enzyme and has the active site in Cys^{250}.

Identification of a novel protein-conjugating enzyme, Ufc1

The LC–MS/MS analysis revealed CGI-126 protein as another Uba5 interacting protein. CGI-126 is a protein of 167-amino-acid residues with a predicted molecular mass of 19.4 kDa. This protein is also conserved in multicellular organisms, like Uba5 and Ufm1 (Figure 4A). The C-terminal half of human CGI-126 has a high identity across species as shown in Figure 4A. CGI-126 has a highly conserved region, for example, residues 113–126, with limited similarity to the region of Ubc's that encodes an active site Cys residue capable of forming a thioester bond (Figure 4A). We assumed that this protein may be an E2-like conjugating enzyme for Ufm1 and thus named it Ufm1-conjugating enzyme 1 (Ufc1). If Ufc1 is an authentic E2 enzyme for Ufm1, it is expected to form an intermediate complex with Ufm1 via a thioester linkage. To test this possibility in the same way as Uba5, we mutated the predicted active site Cys residue within Ufc1 (Figure 4A, Cys^{116}) to Ser. We expressed Flag-Ufc1 or Flag-Ufc1^{C116S} (a presumptive active site Cys at position 116 was replaced by Ser) in combination with Myc-Ufm1 or Myc-Ufm1ΔC3 in HEK293 cells. Flag-Ufc1^{C116S} formed a stable intermediate band when coexpressed with Myc-Ufm1 (Figure 4B, lane 8), but not alone or with Myc-Ufm1ΔC3 (Figure 4B, lanes 7 and 9). To ascertain that this is the Flag-Ufc1^{C116S}–Myc-Ufm1 intermediate, Flag-Ufc1^{C116S} was immunoprecipitated and blotted with anti-Myc antibody (Figure 4C). Indeed, Myc-Ufm1, but not Myc-Ufm1ΔC3, formed a complex with Flag-Ufc1^{C116S} (Figure 4C, lanes 5 and 6, top and bottom panels). Note that Flag-Ufc1^{C116S} intermediate with a faster electrophoretic mobility than the Flag-Ufc1^{C116S}–Myc-Ufm1 complex is presumably the intermediate with the endogenous Ufm1 (Figure 4C, lanes 4–6, upper panel). These results indicate that Ufc1 forms an intermediate with Ufm1 *in vivo*.

To confirm that Ufc1 is indeed an E2-like enzyme that conjugates with Ufm1 *via* a thioester linkage, we conducted an *in vitro* Ufm1 conjugation assay. Recombinant GST-Uba5, GST-Ufc1, and GST-Ufm1ΔC2 were mixed and incubated in the presence of ATP. GST-Ufc1^{C116A} mutant and GST-Ufm1ΔC3 were used as negative controls. Under nonreducing conditions, an ~70 kDa band corresponding to GST-Ufm1ΔC2–GST-Ufc1 intermediate was observed (Figure 4D, lane 4). This product was not formed at reducing conditions, or when any of the components was omitted from the reaction (Figure 4D, lanes 1–3 and 5). GST-tagged Ufc1^{C116A} mutant could not form the intermediate, suggesting that Cys116 is indeed the active site (Figure 4D, lane 7). GST-Ufm1ΔC3 was again unable to form the intermediate complex in this reaction (Figure 4D, lane 9). Taken together, we concluded that Ufc1 functions as an Ufm1-conjugating enzyme and has the active site in Cys^{116}.

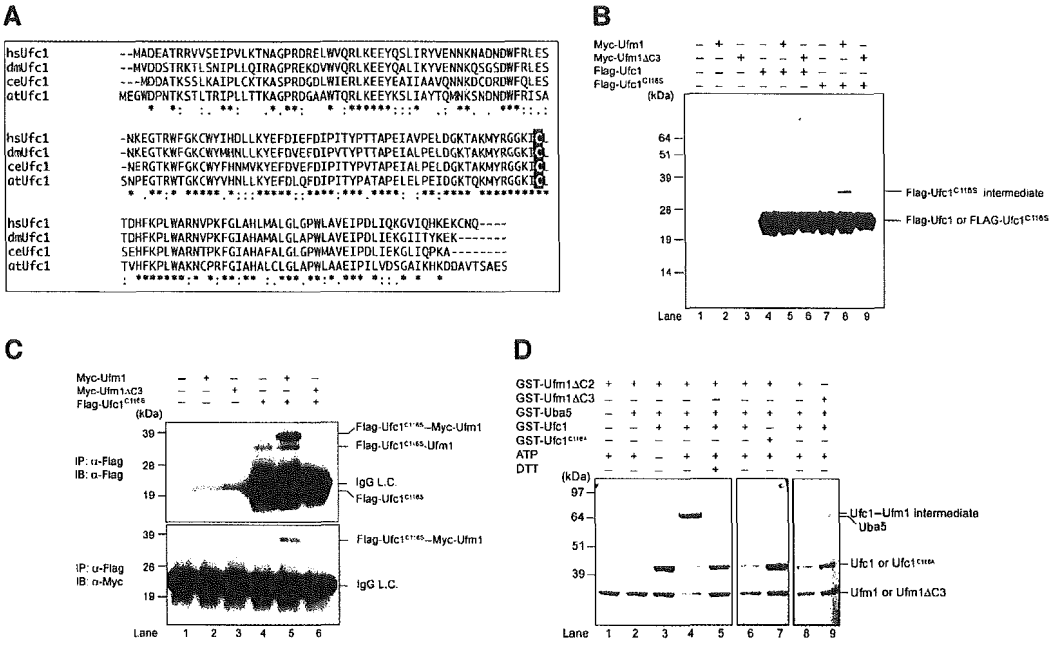

Figure 4 Ufc1, a novel E2-like enzyme. (**A**) Sequence alignment of hsUfc1 and its homologs. The sequence of Ufc1 is available from GenBank™ under the accession number BC005187 (dm, NM_137230; ce, NM_066654; at, BT001180). The homology analysis was performed as described in Figure 1B. The putative active site Cys residue is boxed in black. (**B**) Immunoblotting analysis. Each Myc-tagged Ufm1 (Myc-Ufm1) and Myc-Ufm1ΔC3 was expressed alone (lanes 2 and 3, respectively), and coexpressed with Flag-Ufc1 (lanes 5 and 6, respectively) or Flag-Ufc1^{C116S} (lanes 8 and 9, respectively). Each Flag-Ufc1 and Flag-Ufc1^{C116S} was also expressed alone (lanes 4 and 7, respectively). The cell lysates were subjected to SDS–PAGE and analyzed by immunoblotting with anti-Flag antibody. The bands corresponding to Flag-Ufc1, Flag-Ufc1^{C116S}, and Flag-Ufc1^{C116S} intermediates are indicated on the right. (**C**) Immunoblotting analysis after immunoprecipitation. Each Myc-Ufm1 and Myc-Ufm1ΔC3 was expressed alone (lanes 2 and 3, respectively), and coexpressed with Flag-Ufc1^{C116S} (lanes 5 and 6, respectively). Flag-Ufc1^{C116S} was also expressed alone (lane 4). The cell lysates were immunoprecipitated with anti-Flag antibody. The resulting immunoprecipitates were subjected to SDS–PAGE and analyzed by immunoblots with anti-Flag and anti-Myc antibodies. The bands corresponding to Flag-Ufc1^{C116S}, Flag-Ufc1^{C116S}–endogenous Ufm1, and Flag-Ufc1^{C116S}–Myc-Ufm1 intermediates are indicated. (**D**) *In vitro* thioester bond formation assay of Ufm1 by Ufc1. Purified recombinant GST-Ufm1ΔC2 (2 μg) (lanes 1–8) was incubated for 30 min at 25°C with the following: purified recombinant GST-Uba5 (0.2 μg) (lanes 2–9), GST-Ufc1 (2 μg) (lanes 3–6, 8, and 9), GST-Ufc1^{C116S} (2 μg) (lane 7), and 5 mM ATP (lanes 1, 2, and 4–9). Lane 9 was conducted similar to lane 8, except that GST-Ufm1ΔC3 was used instead of GST-Ufm1ΔC2. Reactions were then incubated with SDS loading buffer lacking reducing agent (lanes 1–4 and 6–9) or containing 100 mM DTT (lane 5). The presence or absence of various components is indicated above the lanes. The bands corresponding to free GST-Ufm1ΔC2 (mature Ufm1), GST-Ufm1ΔC3, GST-Uba5, GST-Ufc1, GST-Ufc1^{C116S}, and GST-Ufc1–GST-Ufm1ΔC2 thioester product are indicated on the right.

Conjugation of Ufm1 to cellular protein(s)

We next examined whether Ufm1 conjugates to the target protein(s) in cells. To this end, we expressed Flag- and 6xHis-tagged Ufm1 constructs in HEK293 cells, and purified them under denaturing conditions by Ni^{2+} beads. The resulting precipitates were then analyzed by immunoblotting with anti-Flag antibody. When FlagHis-Ufm1-HA (proUfm1) or FlagHis-Ufm1ΔC2 (mature form) was expressed, several proteins with sizes of about 28, 38, and 47 kDa were detected, in addition to the 10 kDa corresponding to free FlagHis-Ufm1ΔC2 (Figure 5A, lanes 2 and 4). These bands were not detected by FlagHis-Ufm1^{G83A}-HA and FlagHis-Ufm1ΔC3, suggesting that both C-terminal cleavage and C-terminal Gly residue are required for the conjugation reaction (Figure 5A, lanes 3 and 6). Moreover, these protein bands were resistant to reducing agents, such as DTT and β-mercaptoethanol. These results indicate that Ufm1 is covalently attached to some target proteins, probably through an isopeptide bond between the C-terminal Gly^{83} of Ufm1 and a Lys residue in the cellular proteins. It is of note that FlagHis-Ufm1^{G83A} mutant with exposed C-terminal Ala instead of Gly can conjugate to target proteins (Figure 5A, lane 5), consistent with the previous report on ubiquitin and SUMO (Hodgins *et al*, 1992; Kamitani *et al*, 1997). Since C-terminal Gly to Ala mutation confers resistance to the Ufm1 processing, the conjugates with FlagHis-Ufm1^{G83A} mutant may be more stable than those with FlagHis-Ufm1ΔC2 (Figure 5A, compare lanes 4 and 5). These results suggest that the Ufm1 conjugation is also a reversible reaction.

We further investigated the expression of Ufm1 and its conjugated proteins in mouse tissues using anti-Ufm1 serum. Ufm1 was widely expressed in all tissues examined, such as brain, heart, lung, liver, and kidney (Figure 5B, left panel). In addition, several bands with striking similarity to proteins detected in HEK293 cells were observed. These bands were not detected by preimmune or preabsorbed antisera (Figure 5B, right panel), suggesting that they are likely the Ufm1 conjugates. Although the intensity of each band varied among tissues and HEK293 cells, 28 and 38 kDa proteins were commonly detected. The 70-kDa band observed in all tissues was also detected faintly in HEK293 cells (Figure 5A, lane 5). The 47-kDa band observed in HEK293 cells was not clear. These protein bands were resistant to reducing agents, such as DTT and β-mercaptoethanol, indicating that Ufm1 covalently attaches to cellular proteins like other Ubl proteins. The targets of Ufm1 appeared to be common in a variety

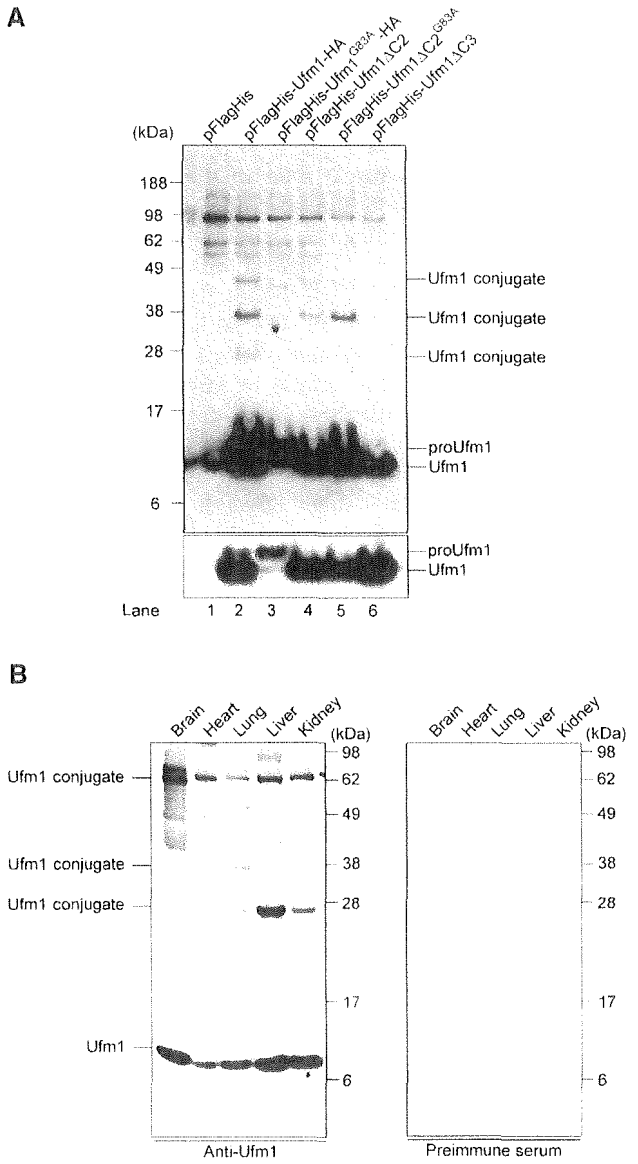

Figure 5 Formation of a covalent protein conjugate(s) with Ufm1 in HEK293 cells and mouse tissues. (**A**) Ufm1 conjugates in human HEK293 cells. HEK293 cells were transfected with FlagHis-Ufm1-HA, FlagHis-Ufm1^{G83A}-HA, FlagHis-Ufm1ΔC2, FlagHis-Ufm1ΔC2^{G83A}, or FlagHis-Ufm1ΔC3 expression plasmids. These cells were lysed under denaturing conditions, and the lysates were precipitated with Ni^{2+} beads. The precipitates were subjected to SDS–PAGE and analyzed by immunoblotting with anti-Flag antibody. The bottom panel shows the short exposure of the upper panel. The bands corresponding to mature Ufm1, proUfm, and Ufm1 conjugates are indicated on the right. (**B**) Ufm1 conjugates in various mouse tissues. Homogenates from mouse tissues as indicated were prepared and subjected to SDS–PAGE and analyzed by immunoblotting with anti-Ufm1 serum (left panel) or preimmune serum (right panel). The bands corresponding to Ufm1 and conjugates between Ufm1 and target proteins are indicated on the left.

of tissues. These results suggest the universal roles of Ufm1 in the regulation of cellular function in multicellular organisms.

Subcellular localization of Ufm1 in HeLa cells

We finally examined the subcellular distribution of Ufm1 in HeLa cells. Immunocytochemical analysis using anti-Ufm1

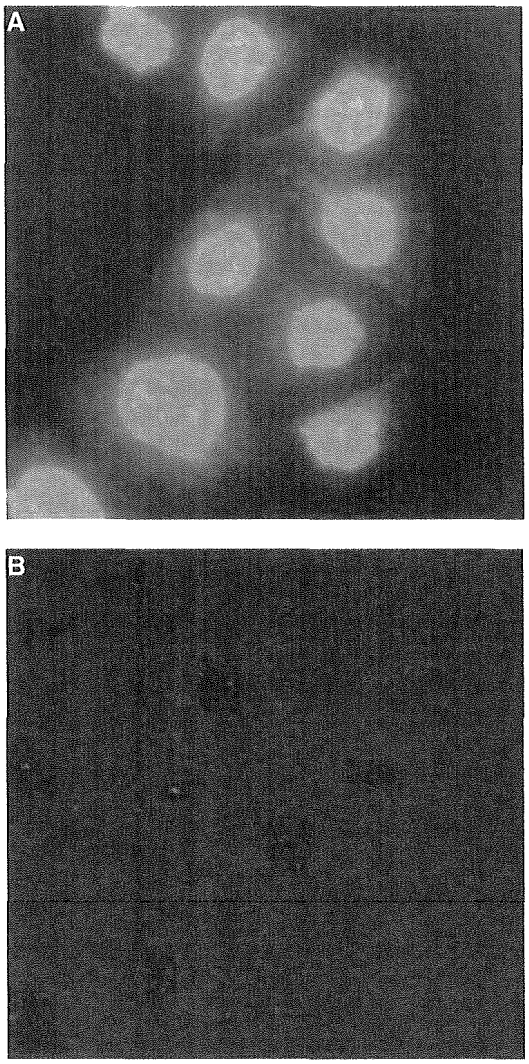

Figure 6 Intracellular distribution of Ufm1 in HeLa cells. (**A**) HeLa cells were seeded on coverslips 24 h before fixation for immunostaining. Ufm1 was detected with anti-Ufm1 serum and visualized with Alexa 488 nm anti-rabbit antibody. (**B**) Immunocytochemical analysis was conducted as for (A), except that preimmune serum was used. Cells were observed using a fluorescence microscope. Magnification, ×400.

serum revealed that Ufm1 was predominantly localized in the nucleus and diffusely in the cytoplasm (Figure 6A). These staining patterns were not observed when anti-Ufm1 serum had been preadsorbed with excess amounts of recombinant Ufm1 protein or preimmune serum was used instead of anti-Ufm1 serum (Figure 6B). Moreover, Ufm1 localization in the cytoplasm and nucleus was similar to the localization of exogenously expressed GFP-tagged Ufm1 in HeLa cells (data not shown). In the nucleus, strong immunoreactivity to anti-Ufm1 serum was observed as a dot-like structure. Although such dots-like structures were detected by preimmune serum, those intensities were weak. Thus, some of these dot-like structures may represent conjugates of Ufm1.

Discussion

In the present study, we reported that Ufm1 acts as a new post-translational UBL modifier, based on the following

criteria: (1) It is a small protein of 9.1 kDa with a ubiquitin-fold structure. (2) Ufm1 is synthesized in a precursor form, and the extra amino-acid residues at the C-terminal side need to be processed to expose the Gly residue. (3) The C-terminal processing and exposure of glycine residue are essential to the formation of Ufm conjugates in the cells. (4) Ufm1 has specific E1-like (Uba5) and E2-like (Ufc1) enzymes for activation and conjugation, respectively. Intriguingly, many UBL modifiers are evolutionarily conserved from yeast to human, except interferon-inducible UBL modifiers, such as UCRP/ISG15, Fat10, and Fau1/MNSFβ (Nakamura *et al*, 1995; D'Cunha *et al*, 1996; Liu *et al*, 1999). Ufm1, Uba5, and Ufc1 found in the present study are conserved in various multicellular organisms (Figures 1B, 2A, and 4A), but not in both budding and fission yeasts, suggesting that they all have been generated by coevolution.

We identified Uba5 as an E1 enzyme for Ufm1. This enzyme is relatively small compared to Uba1, that is, an E1 for ubiquitin (Figure 1A). In the *in vitro* assay, the recombinant Uba5 protein formed a thioester linkage with recombinant Ufm1 (Figure 3C) and transferred the activated Ufm1 to recombinant Ufc1 (an E2 enzyme) (Figure 4D), indicating that Uba5 can activate Ufm1 as a single molecule. This is in marked contrast to other E1s such as Uba2 and Uba3, which retain obvious similarities to the C-terminal half of Uba1 but require the formation of heterodimer complexes with respective partner molecules, AOS1 and APP-BP1, respectively, with similarities to the N-terminal half of Uba1 (Johnson *et al*, 1997; Liakopoulos *et al*, 1998; Osaka *et al*, 1998). Another E1-like enzyme, Uba4 that activates Urm1, is of similar size to Uba5 (Furukawa *et al*, 2000), but it remains unknown whether Uba4 acts as a single molecule or needs a partner subunit. The homology of Uba5 to Uba1 is less than those of Uba2 and Uba3, except their ThiF domain conserved in E1s, and thus it is likely that Uba5 may uniquely activate Ufm1, differing from other E1s such as Uba1, Uba2/AOS1, and Uba3/APP-BP1. Thus, although the structure of APP-BP1/Uba3 heterodimer is determined and the mechanism by which E1s activate their cognate UBLs was proposed (Walden *et al*, 2003a, b), the weak homology of Uba5 with other E1s hampered the computer-assisted structural analysis. To clarify this issue, structural analysis of Uba5 is required. This issue is currently under investigation in our laboratories. So far, most E1-like enzymes activate single species of UBL protein, although Atg7 is exception, which can activate both Atg8 and Atg12 (Mizushima *et al*, 1998; Tanida *et al*, 1999; Ichimura *et al*, 2000). A total of 10 E1-like enzymes can be identified in the human genome by computer analysis. Considering the limited number of E1-like proteins, it is possible that some E1-like proteins can activate a distinct set of UBL proteins. Whether or not Uba5 is capable of activating proteins other than Ufm1 remains to be clarified.

There are more than a dozen of E2 family genes in human genomes. In the budding yeast, 13 different E2s, namely Ubc1–Ubc13, have been documented and functionally characterized. Functionally, most of them catalyze the conjugation of ubiquitin, except that Ubc9 and Ubc12 are for SUMO and NEDD8/Rub1, respectively (Johnson and Blobel, 1997; Lammer *et al*, 1998; Osaka *et al*, 1998). In addition, in the autophagic pathway, Atg3 and Atg10 are both E2 enzymes for Atg8 and Atg12, respectively, but they do not have obvious sequence similarities to known Ubc's, except for a short region encompassing an active Cys residue (Shintani *et al*, 1999; Ichimura *et al*, 2000). Similarly, Ufc1 is a unique E2-like enzyme with no obvious sequence homology with other E2s, except approximately 10 amino-acid residues encompassing the active site Cys residue.

In assessing the biological roles of the Ufm1-modifying system, characterization of the target molecule(s) is of particular importance. Regarding this issue, we identified several putative proteins that are conjugated with Ufm1 in human HEK293 cells and various mouse tissues. It is noteworthy that the sizes of these bands (28, 38, 47 kDa) increase by 10 kDa, which is consistent with the size of Ufm1. Considering that several Ubl modifiers can attach to target proteins as a polymer, it is possible that these bands correspond to multi- or poly-Ufm1 conjugates. In fact, Ufm1 has six Lys residues. Whether Ufm1 is conjugated to several distinct proteins or multiple Lys residues in a single target or polymerized in a single Lys residue awaits future study. Unfortunately, we could not identify the protein, and detailed analysis of the cellular function of Ufm1 conjugation awaits future study. It was recently reported that Uba5 is induced by certain reagents that induce stress in the endoplasmic reticulum (ER), a so-called 'unfolded protein response' (Harding *et al*, 2003). However, we could not observe the induction of Uba5, Ufc1, and Ufm1 by treatment with various compounds known to induce ER stress in mammalian cells (data not shown). In addition, exposure to other stresses including high temperature or heavy metals also did not induce the appearance of obvious new conjugation band(s) of Ufm1, by immunoblot analysis. Further studies on the biological roles of the Ufm1 conjugation pathway are under investigation in our laboratories.

Materials and methods

DNA construction

The cDNA encoding human Uba5 was obtained by PCR from human liver cDNA with the Uba5-s5′ primer (5′-CGGAGGGATCCC CATGGCGGAGTCTGTGGAG-3′) and the Uba5-r3′ primer (5′-CAGTCCTCGAGCTACATATTCTTCATTTT-3′). It was then subcloned into pcDNA3 vector (Invitrogen, San Diego, CA). A point mutation for Cys at position 250 to Ser or Ala was generated by PCR-based site-directed mutagenesis. The Flag tag was introduced at the N-terminus of Uba5 or Uba5^{C250S}. Similarly, cDNA encoding human Ufm1 was amplified by PCR from human liver cDNA with the Ufm1-s5′ primer (5′-TTCCGGGATCCCCATGTCGAAGGTTTCCTTT-3′) and the Ufm1-r3′ primer (5′-AGTAGCTCGAGTTAACAACTTCCAA CACGAT-3′), and subcloned into pcDNA3 vector. The Flag, FlagHis, or Myc tags were introduced at the N-terminus of Ufm1. The HA tag was introduced at the C-terminus of Ufm1. The C-terminal deletion mutants of Ufm1 named Ufm1ΔC2 and Ufm1ΔC3, encoding amino acids 1–83 and 1–82, respectively, were generated by PCR. A point mutation for Gly at position 83 to Ala of Ufm1 and Ufm1ΔC2 (Ufm1^{G83A} and Ufm1ΔC2^{G83A}, respectively) was generated by PCR-based site-directed mutagenesis. The cDNA encoding human Ufc1 was obtained by PCR from human liver cDNA with the Ufc1-s5′ primer (5′-GCCCTGGATCCAGATGGCGGATGAAGCCACG-3′) and the Ufc1-r3′ primer (5′-TTCTCGAGTCATTGGTTGCATTTCTCTT-3′). It was then subcloned into pcDNA3 vector. A point mutation for Cys at position 116 to Ser or Ala was generated by PCR-based site-directed mutagenesis. The Flag tag was introduced at the N-terminus of Ufc1 and Ufc1^{C116S}. To express GST-fused Ufm1ΔC2, Ufm1ΔC3, Uba5, Uba5^{C250A}, Ufc1, and Ufc1^{C116A} in *E. coli*, these cDNAs were subcloned into pGEX-6p vector (Amersham Biosciences). All mutations mentioned above were confirmed by DNA sequencing.

Cell culture and transfection

Media and reagents for cell culture were purchased from Life Technologies (Grand Island, NY). HEK293 cells were grown in Dulbecco's modified Eagle's medium (DMEM) containing 10% fetal calf serum (FCS), 5 U/ml penicillin, and 50 μg/ml streptomycin. HEK293 cells at subconfluence were transfected with the indicated plasmids using Fugene 6 reagent (Roche Molecular Biochemicals, Mannheim, Germany). Cells were analyzed at 20–24 h after transfection.

Immunological analysis

For immunoblot analysis, cells were lysed with ice-cold TNE buffer (10 mM Tris–HCl, pH 7.5, 1% Nonidet P-40, 150 mM NaCl, 1 mM ethylenediaminetetraacetic acid (EDTA), and protease inhibitors) and the lysates were separated by SDS–PAGE (12% gel or 4–12% gradient gel) and transferred to a polyvinylidene difluoride (PVDF) membrane. Mouse monoclonal anti-Flag antibody (M2; Sigma Chemical Co., St Louis, MO), anti-HA antibody (F7; Santa Cruz Biotechnology, Santa Cruz, CA), and rabbit polyclonal anti-Myc antibody (N14; Santa Cruz) were used for immunodetection. Development was performed by the Western lighting detection methods.

For immunoprecipitation analysis, cells were lysed by 200 μl of TNE, and the lysate was then centrifuged at 10 000 *g* for 10 min at 4°C to remove debris. In the next step, 800 μl of TNE and 30 μl of M2-agarose (Sigma) were added to the lysate, and the mixture was mixed under constant rotation for 12 h at 4°C. The immunoprecipitates were washed five times with ice-cold TNE. The complex was boiled for 10 min in SDS sample buffer in the presence of β-mercaptoethanol to elute proteins and centrifuged at 10 000 *g* for 10 min at 4°C. The supernatant was subjected to SDS–PAGE, transferred to PVDF membrane, and analyzed by immunoblots with anti-Flag (M2) or anti-Myc (N14) antibody.

For purification of 6xHis-tagged proteins under denaturing conditions, cells were lysed by 1 ml of denaturing lysis buffer (8 M urea, 0.1 M NaH_2PO_4, and 0.01 M Tris–HCl, pH 8.0) in the presence of 20 mM *N*-ethylmaleimide as an inhibitor of isopeptidases, and the lysate was sonicated briefly and then centrifuged at 10 000 *g* for 10 min at room temperature to remove debris. Then, 30 μl of Ni-NTA Superflow (QIAGEN) was added to the lysate, and the mixture was shaken under constant rotation for 30 min at room temperature. The precipitates were washed five times with denaturing wash buffer (8 M urea, 0.1 M NaH_2PO_4, and 0.01 M Tris–HCl, pH 5.9). To elute proteins, elution buffer (8 M urea, 0.1 M NaH_2PO_4, and 0.01 M Tris–HCl, pH 4.5) was added to the complex, and the mixture was centrifuged at 10 000 *g* for 10 min at room temperature. The resulting supernatant was subjected to SDS–PAGE, transferred to PVDF membrane, and analyzed by immunoblots with anti-Flag (M2).

Freshly isolated tissues from mice were homogenized in lysis buffer (50 mM Tris–HCl, pH 7.5, 1% SDS, 5 mM EDTA, and 10 mM β-mercaptoethanol) using potter-Elvehjem homogenizer. The homogenate was centrifuged at 10 000 *g* for 10 min to remove debris. The resulting supernatant was subjected to SDS–PAGE, transferred to PVDF membrane, and analyzed by immunoblotting with anti-Ufm1 or preimmune serum. The anti-Ufm1 polyclonal antibody was raised in rabbits using the recombinant protein produced in *E. coli* as an antigen.

In vitro thioester formation assay

Recombinant GST-Ufm1ΔC2, GST-Ufm1ΔC3, GST-Uba5, GST-Uba5^{C250A}, GST-Ufc1, and GST-Ufc1^{C116A} (tagged N-terminally with GST) were produced in *E. coli* and recombinant proteins were purified by chromatography on glutathione sepharose 4B (Amersham Biosciences). After elution of proteins from the beads, the preparations were dialyzed against 50 mM BisTris (pH 6.5), 100 mM NaCl, 10 mM $MgCl_2$, and 0.1 mM DTT (reaction buffer). Most thioester formation reactions contained reaction buffer with 4 μg GST-Ufm1ΔC2 or GST-Ufm1ΔC3 and some of the following: 5 mM ATP, 2 or 0.2 μg GST-Uba5 or GST-Uba5^{C250A}, and 4 μg GST-Ufc1 or GST-Ufc1^{C116A}. Reactions were incubated for 30 min at 25°C and stopped by the addition of SDS-containing loading buffer either lacking reducing agent or containing 100 mM DTT, followed by a 10 min incubation at 37°C, SDS–PAGE (4–12% acrylamide gradient) and Coomassie brilliant blue staining.

Protein identification by LC–MS/MS analysis

The Uba5-associated complexes were digested with *Achromobacter* protease I and the resulting peptides were analyzed using a nanoscale LC–MS/MS system as described previously (Natsume *et al*, 2002). The peptide mixture was applied to a Mightysil-PR-18 (1 μm particle, Kanto Chemical) frit-less column (45 mm × 0.150 mm ID) and separated using a 0–40% gradient of acetonitrile containing 0.1% formic acid over 30 min at a flow rate of 50 nl/min. Eluted peptides were sprayed directly into a quadropole time-of-flight hybrid mass spectrometer (Q-Tof *Ultima*, Micromass, Manchester, UK). MS and MS/MS spectra were obtained in a data-dependent mode. Up to four precursor ions above an intensity threshold of 10 counts/s were selected for MS/MS analyses from each survey scan. All MS/MS spectra were searched against protein sequences of Swiss Prot and RefSeq (NCBI) using batch processes of Mascot software package (Matrix Science, London, UK). The criteria for match acceptance were the following: (1) When the match score was 10 over each threshold, identification was accepted without further consideration. (2) When the difference of score and threshold was lower than 10, or when proteins were identified based on a single matched MS/MS spectrum, we manually confirmed the raw data prior to acceptance. (3) Peptides assigned by less than three y series ions and peptides with +4 charge state were all eliminated regardless of their scores.

Immunofluorescence

HeLa cells grown on glass coverslips were fixed in 4% paraformaldehyde (PFA) in PBS for 15 min, and permeabilized with 0.2% (vol/vol) Triton X-100 in PBS for 30 min. After permeabilization, the cells were blocked for 30 min with 5% (vol/vol) normal goat serum in PBS, incubated for 1 h at 37°C with anti-Ufm1 serum or preimmune serum, washed with PBS, and incubated for 30 min with Alexa 488 nm anti-rabbit antibodies (Molecular Probes). The coverslips were washed and mounted on slides. Fluorescence images were obtained using a fluorescence microscope (DMIRE2; Leica) equipped with a cooled charge-coupled device camera (CTR MIC; Leica). Pictures were taken using Leica Qfluoro software (Leica).

Acknowledgements

We thank T Mizushima (Nagoya University) for the computer-assisted structural modeling of human Ufm1. This work was supported in part by Grants-in-Aid from the Ministry of Education, Culture, Sports, Science and Technology of Japan.

References

Bonifacino JS, Weissman AM (1998) Ubiquitin and the control of protein fate in the secretory and endocytic pathways. *Annu Rev Cell Dev Biol* **14:** 19–57

Cort JR, Chiang Y, Zheng D, Montelione GT, Kennedy MA (2002) NMR structure of conserved eukaryotic protein ZK652.3 from *C. elegans*: a ubiquitin-like fold. *Proteins* **48:** 733–736

D'Cunha J, Knight Jr E, Haas AL, Truitt RL, Borden EC (1996) Immunoregulatory properties of ISG15, an interferon-induced cytokine. *Proc Natl Acad Sci USA* **93:** 211–215

Furukawa K, Mizushima N, Noda T, Ohsumi Y (2000) A protein conjugation system in yeast with homology to biosynthetic enzyme reaction of prokaryotes. *J Biol Chem* **275:** 7462–7465

Glickman MH, Ciechanover A (2002) The ubiquitin-proteasome proteolytic pathway: destruction for the sake of construction. *Physiol Rev* **82:** 373–428

Harding HP, Zhang Y, Zeng H, Novoa I, Lu PD, Calfon M, Sadri N, Yun C, Popko B, Paules R, Stojdl DF, Bell JC, Hettmann T, Leiden JM, Ron D (2003) An integrated stress response regulates amino

acid metabolism and resistance to oxidative stress. *Mol Cell* **11:** 619–633

Hershko A, Ciechanover A (1998) The ubiquitin system. *Annu Rev Biochem* **67:** 425–479

Hodgins RR, Ellison KS, Ellison MJ (1992) Expression of a ubiquitin derivative that conjugates to protein irreversibly produces phenotypes consistent with a ubiquitin deficiency. *J Biol Chem* **267:** 8807–8812

Ichimura Y, Kirisako T, Takao T, Satomi Y, Shimonishi Y, Ishihara N, Mizushima N, Tanida I, Kominami E, Ohsumi M, Noda T, Ohsumi Y (2000) A ubiquitin-like system mediates protein lipidation. *Nature* **408:** 488–492

Jentsch S, Pyrowolakis G (2000) Ubiquitin and its kin: how close are the family ties? *Trends Cell Biol* **10:** 335–342

Johnson ES, Blobel G (1997) Ubc9p is the conjugating enzyme for the ubiquitin-like protein Smt3p. *J Biol Chem* **272:** 26799–26802

Johnson ES, Schwienhorst I, Dohmen RJ, Blobel G (1997) The ubiquitin-like protein Smt3p is activated for conjugation to other proteins by an Aos1p/Uba2p heterodimer. *EMBO J* **16:** 5509–5519

Kabeya Y, Mizushima N, Ueno T, Yamamoto A, Kirisako T, Noda T, Kominami E, Ohsumi Y, Yoshimori T (2000) LC3, a mammalian homologue of yeast Apg8p, is localized in autophagosome membranes after processing. *EMBO J* **19:** 5720–5728

Kamitani T, Nguyen HP, Yeh ET (1997) Preferential modification of nuclear proteins by a novel ubiquitin-like molecule. *J Biol Chem* **272:** 14001–14004

Klionsky DJ, Cregg JM, Dunn Jr WA, Emr SD, Sakai Y, Sandoval IV, Sibirny A, Subramani S, Thumm M, Veenhuis M, Ohsumi Y (2003) A unified nomenclature for yeast autophagy-related genes. *Dev Cell* **5:** 539–545

Klionsky DJ, Emr SD (2000) Autophagy as a regulated pathway of cellular degradation. *Science* **290:** 1717–1721

Komatsu M, Tanida I, Ueno T, Ohsumi M, Ohsumi Y, Kominami E (2001) The C-terminal region of an Apg7p/Cvt2p is required for homodimerization and is essential for its E1 activity and E1–E2 complex formation. *J Biol Chem* **276:** 9846–9854

Lammer D, Mathias N, Laplaza JM, Jiang W, Liu Y, Callis J, Goebl M, Estelle M (1998) Modification of yeast Cdc53p by the ubiquitin-related protein rub1p affects function of the SCFCdc4 complex. *Genes Dev* **12:** 914–926

Liakopoulos D, Doenges G, Matuschewski K, Jentsch S (1998) A novel protein modification pathway related to the ubiquitin system. *EMBO J* **17:** 2208–2214

Liu YC, Pan J, Zhang C, Fan W, Collinge M, Bender JR, Weissman SM (1999) A MHC-encoded ubiquitin-like protein (FAT10) binds noncovalently to the spindle assembly checkpoint protein MAD2. *Proc Natl Acad Sci USA* **96:** 4313–4318

Mizushima N, Noda T, Yoshimori T, Tanaka Y, Ishii T, George MD, Klionsky DJ, Ohsumi M, Ohsumi Y (1998) A protein conjugation system essential for autophagy. *Nature* **395:** 395–398

Nakamura M, Xavier RM, Tsunematsu T, Tanigawa Y (1995) Molecular cloning and characterization of a cDNA encoding monoclonal nonspecific suppressor factor. *Proc Natl Acad Sci USA* **92:** 3463–3467

Natsume T, Yamauchi Y, Nakayama H, Shinkawa T, Yanagida M, Takahashi N, Isobe T (2002) A direct nanoflow liquid chromatography–tandem mass spectrometry system for interaction proteomics. *Anal Chem* **74:** 4725–4733

Ohsumi Y (2001) Molecular dissection of autophagy: two ubiquitin-like systems. *Nat Rev Mol Cell Biol* **2:** 211–216

Osaka F, Kawasaki H, Aida N, Saeki M, Chiba T, Kawashima S, Tanaka K, Kato S (1998) A new NEDD8-ligating system for cullin-4A. *Genes Dev* **12:** 2263–2268

Pickart CM (2001) Mechanisms underlying ubiquitination. *Annu Rev Biochem* **70:** 503–533

Schwartz DC, Hochstrasser M (2003) A superfamily of protein tags: ubiquitin, SUMO and related modifiers. *Trends Biochem Sci* **28:** 321–328

Shintani T, Mizushima N, Ogawa Y, Matsuura A, Noda T, Ohsumi Y (1999) Apg10p, a novel protein-conjugating enzyme essential for autophagy in yeast. *EMBO J* **18:** 5234–5241

Tanaka K, Suzuki T, Chiba T (1998) The ligation systems for ubiquitin and ubiquitin-like proteins. *Mol Cells* **8:** 503–512

Tanida I, Komatsu M, Ueno T, Kominami E (2003) GATE-16 and GABARAP are authentic modifiers mediated by Apg7 and Apg3. *Biochem Biophys Res Commun* **300:** 637–644

Tanida I, Mizushima N, Kiyooka M, Ohsumi M, Ueno T, Ohsumi Y, Kominami E (1999) Apg7p/Cvt2p: a novel protein-activating enzyme essential for autophagy. *Mol Biol Cell* **10:** 1367–1379

Varshavsky A (1997) The ubiquitin system. *Trends Biochem Sci* **22:** 383–387

Walden H, Podgorski MS, Huang DT, Miller DW, Howard RJ, Minor Jr DL, Holton JM, Schulman BA (2003a) The structure of the APPBP1–UBA3–NEDD8–ATP complex reveals the basis for selective ubiquitin-like protein activation by an E1. *Mol Cell* **12:** 1427–1437

Walden H, Podgorski MS, Schulman BA (2003b) Insights into the ubiquitin transfer cascade from the structure of the activating enzyme for NEDD8. *Nature* **422:** 330–334

Yeh ET, Gong L, Kamitani T (2000) Ubiquitin-like proteins: new wines in new bottles. *Gene* **248:** 1–14

nature
structural &
molecular biology

Structural basis of sugar-recognizing ubiquitin ligase

Tsunehiro Mizushima[1,2], Takeshi Hirao[3], Yukiko Yoshida[2,4], Soo Jae Lee[5], Tomoki Chiba[2], Kazuhiro Iwai[4,6], Yoshiki Yamaguchi[3,4], Koichi Kato[3,4,7], Tomitake Tsukihara[5] & Keiji Tanaka[2]

Reprinted from nature structural & molecular biology, volume 11, april 2004

nature
structural &
molecular biology

Structural basis of sugar-recognizing ubiquitin ligase

Tsunehiro Mizushima[1,2], Takeshi Hirao[3], Yukiko Yoshida[2,4], Soo Jae Lee[5], Tomoki Chiba[2], Kazuhiro Iwai[4,6], Yoshiki Yamaguchi[3,4], Koichi Kato[3,4,7], Tomitake Tsukihara[5] & Keiji Tanaka[2]

SCF^{Fbs1} is a ubiquitin ligase that functions in the endoplasmic reticulum (ER)-associated degradation pathway. Fbs1/Fbx2, a member of the F-box proteins, recognizes high-mannose oligosaccharides. Efficient binding to an N-glycan requires di-*N*-acetylchitobiose (chitobiose). Here we report the crystal structures of the sugar-binding domain (SBD) of Fbs1 alone and in complex with chitobiose. The SBD is composed of a ten-stranded antiparallel β-sandwich. The structure of the SBD–chitobiose complex includes hydrogen bonds between Fbs1 and chitobiose and insertion of the methyl group of chitobiose into a small hydrophobic pocket of Fbs1. Moreover, NMR spectroscopy has demonstrated that the amino acid residues adjoining the chitobiose-binding site interact with the outer branches of the carbohydrate moiety. Considering that the innermost chitobiose moieties in N-glycans are usually involved in intramolecular interactions with the polypeptide moieties, we propose that Fbs1 interacts with the chitobiose in unfolded N-glycoprotein, pointing the protein moiety toward E2 for ubiquitination.

So far, numerous studies have emphasized the physiological importance of the ubiquitin- and proteasome-mediated proteolytic pathway[1]. The ubiquitination reaction is catalyzed by an elaborate cascade system, consisting of activating (E1), conjugating (E2) and ligating (E3) enzymes[1,2]. Of these enzymes, E3 enzymes are considered to exist as molecules with a large diversity and to have a principal role in the selection of target proteins for ubiquitination in a temporally and spatially regulated fashion[3].

One of the best-characterized E3 enzymes is the SCF complex (composed of Skp1, Cul1, Roc1 (also called Rbx1) and an F-box protein), which regulates degradation of a broad range of cellular proteins[4]. The F-box proteins consist of an F-box domain that binds to Skp1, and various C-terminal substrate recognition regions, which are subclassified into a family of proteins named Fbw and Fbl that contain WD40-repeat and leucine-rich repeat (LRR) domains, respectively[5]. In addition, the remaining groups have been provisionally classified as Fbx proteins, which show no homology to any other known proteins[5]. However, we recently discovered a third category of the F-box protein family named Fbs (F-box sugar recognition)/FBG[6], consisting of at least five structurally related proteins including Fbs1 (named originally as Fbx2)[7] and Fbs2/Fbx6b (ref. 8). Fbw and Fbl proteins usually recognize the phosphorylation status of the substrate, and the tertiary structures of some of these proteins, such as Fbw1/βTrCP, Fbw7/Cdc4 and Fbl1/Skp2, have been determined by X-ray crystallography, providing valuable information for determining the molecular recognition mechanisms of target proteins[9–12]. However, the molecular basis underlying the ability of Fbs proteins to recognize target glycoproteins remains to be clarified.

Eukaryotic cells have an abundant and diverse repertoire of N-linked oligosaccharide structures, but the role of N-glycosylation of the proteins remains largely unknown. N-glycans have recently been shown to have an important role in glycoprotein transport and sorting[13,14]. N-glycoproteins are also subjected to 'quality control,' in which aberrant proteins are distinguished from properly folded proteins and retained in the ER[15]. When the improperly folded or incompletely assembled proteins fail to restore their functional states, they are degraded by the ER-associated degradation (ERAD) system, which involves retrograde transfer of proteins from the ER to the cytosol and subsequent degradation mediated by ubiquitin and proteasomes[16]. Recently, we identified the SCF^{Fbs1} as an E3 ubiquitin–ligase complex that ubiquitinates N-linked glycoproteins, serving to clear these glycoproteins in the cytosol of the cell[7]. Fbs1 recognizes N-linked high-mannose oligosaccharides, especially the internal diacetylchitobiose structure[8]. However, the molecular mechanism of the recognition of N-glycans by Fbs1 is unknown at present. To understand the molecular basis of the interaction between Fbs1 and N-glycans, we conducted crystal structural analyses of the SBD of Fbs1 and its complex with chitobiose.

RESULTS

Overall structure of the SBD in Fbs1

The structure of the SBD of Fbs1, as determined at a resolution of 2.0 Å (Table 1), is an ellipsoid composed of a ten-stranded antiparallel β-sandwich with two α-helices (Fig. 1a,b). This structure is

[1]Precursory Research for Embryonic Science and Technology (PRESTO), Japan Science and Technology Agency, Kawaguchi, Saitama 332-0012, Japan. [2]Tokyo Metropolitan Institute of Medical Science, Bunkyo-ku, Tokyo 113-8613, Japan. [3]Department of Structural Biology and Biomolecular Engineering, Graduate School of Pharmaceutical Sciences, Nagoya City University, 3-1 Tanabe-dori, Mizuho-ku, Nagoya 467-8603, Japan. [4]Core Research for Evolutional Science and Technology (CREST), Japan Science and Technology Agency, Saitama 332-0012, Japan. [5]Institute for Protein Research, Osaka University, 3-2 Yamadaoka, Suita, Osaka 565-0871, Japan. [6]Department of Molecular Cell Biology, Graduate School of Medicine, Osaka City University, Osaka 545-8585, Japan. [7]Genomic Sciences Center, RIKEN Yokohama Institute, 1-7-29 Suehiro-cho, Tsurumi-ku, Yokohama 230-0045, Japan. Correspondence should be addressed to K.T. (tanakak@rinshoken.or.jp).

Published online 29 February 2004; doi:10.1038/nsmb732

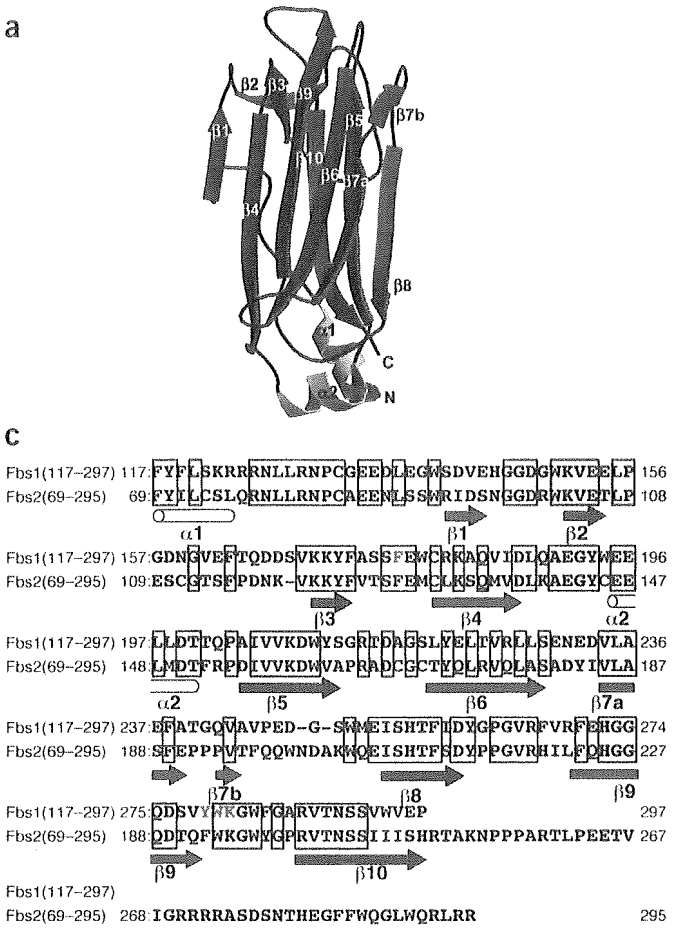

Figure 1 Tertiary structure of SBD in Fbs1. (**a**) Overall structure of SBD of Fbs1 shown as a ribbon diagram. β-strands belonging to S1 and S2 are blue and red, respectively. Loops and helices are black and yellow, respectively. (**b**) A topology diagram of SBD. The α-helices are yellow cylinders labeled α1 and α2. The β-strands are arrows labeled β1–β10. The left and right forms of β-strands correspond to S1 and S2, respectively, as in **a**. N and C, N and C termini, respectively. (**c**) Amino acid sequences of SBD in Fbs1 and corresponding region of Fbs2. Amino acid residues are numbered in the N-to-C direction, for example, from position 117 to position 297 (C-terminal end) of Fbs1, and from 69 to 295 (C-terminal end) of Fbs2. Identical residues are boxed. Secondary structure elements are colored as **a**. Substrate-binding residues are red characters.

completely different from the folds of substrate-binding regions of F-box domains so far reported, including the WD40-repeat domain of CDC4 (ref. 11) and the LRR domain of Skp2 (ref. 12). Strands β1, β4, β6, β7 and β9 form one β-sheet, whereas the other β-sheet consists of strands β2, β3, β5, β8 and β10. These two sheets are named the S1 and S2 sheets, respectively (**Fig. 1a–c**). Strand β7, which is located at one edge of the S1 sheet, is composed of two segments (β7a and β7b) separated by a bent structure. The two α-helices (α1 and α2) lie at one end of the β-sandwich; the α1 helix is at the N terminus and α2 helix is in the loop between β4 and β5. Comparisons of the SBD structure described here with the Protein Data Bank using the Dali server[17] revealed that the SBD is structurally similar to certain lectins, such as the galectin-3 carbohydrate recognition domain[18] and second family 4 carbohydrate-binding modules of xylanase 10A (ref. 19), with r.m.s. deviation values of 2.8 and 2.8 Å, respectively. Indeed, both xylanase and galectin-3 domains are composed of 11-stranded antiparallel β-sandwiches, consisting of 5- and 6-stranded β-sheets, respectively, the overall structures of which resemble that of the SBD, although, in contrast to the SBD, they lack α-helices. Comparing their primary structures, the SBD shows considerable homology to the carbohydrate-binding domain of xylanase 10A, exhibiting amino acid identity of ~20%, whereas no obvious sequence homology was found between SBD and the carbohydrate recognition of galectin-3.

The sugar-binding site

Next, we analyzed the structure of the SBD in complex with chitobiose. We could not obtain SBD crystals in the presence of chitobiose that diffracted to high resolution, so we introduced a C132A mutation in the SBD. The C132A SBD cocrystallized with chitobiose, and the structure of the C132A SBD–chitobiose complex was determined at 2.4 Å resolution (**Fig. 2a** and **Table 1**). The r.m.s. deviation values between SBD and the C132A mutant–chitobiose complex were 0.53 Å and 0.83 Å for the main chain and all atoms, respectively, indicating that the cysteine mutation hardly perturbs the conformation of the wild type SBD. It was also confirmed that this mutation did not alter the interaction and ubiquitination activities of glycoproteins (see **Fig. 3b**).

Chitobiose was clearly located in the difference electron density map (**Fig. 2a**), with *B*-factors as low as those of protein atoms around the chitobiose. The chitobiose in the SBD–chitobiose complex exhibited a *trans* conformation with respect to the *N*-acetyl groups, similar to the structures of a large number of N-glycan-binding proteins[20]. The bound chitobiose formed an intramolecular hydrogen bond between O6 of one GlcNAc(A) residue and O3 of the other GlcNAc(B) residue (**Fig. 2b,c**). The sugar-binding surface consists of two loops: L1 connects strands β3 and β4, and L2 is between strands β9 and β10. The GlcNAc(A) residue stacks on the aromatic ring of Trp280, as is often found in protein-carbohydrate interactions[21,22]. The GlcNAc-Trp280 stacking is stabilized by hydrogen bonds mediated by a water molecule between the O7 of the GlcNAc(A) and Nε1 of Trp280 (**Fig. 2c**), as well as a hydrogen bond between O6 of the GlcNAc(A) and the carbonyl oxygen atom of Lys281. The other GlcNAc(B) residue inserts the methyl group of its *N*-acetyl moiety into a small hydrophobic pocket surrounded by side chains of Phe177, Tyr279 and Lys281 (**Fig. 2a,b**) and forms a hydrogen bond between its hydroxyl and the main chain N atom of Lys281 (**Fig. 2c**). The orientation of the phenyl group of Tyr279 is stabilized by a hydrogen bond with the carboxyl group of Glu178. Upon N-glycoprotein uptake, the SBD swings the side chain of Lys281 (data not shown) and shields the methyl group from the molecular surface. The hydroxyl groups of the chitobiose almost exactly replace two binding site water molecules, which form a hydrogen bond to the backbone O and N of Lys281, respectively (**Fig. 2b,c**).

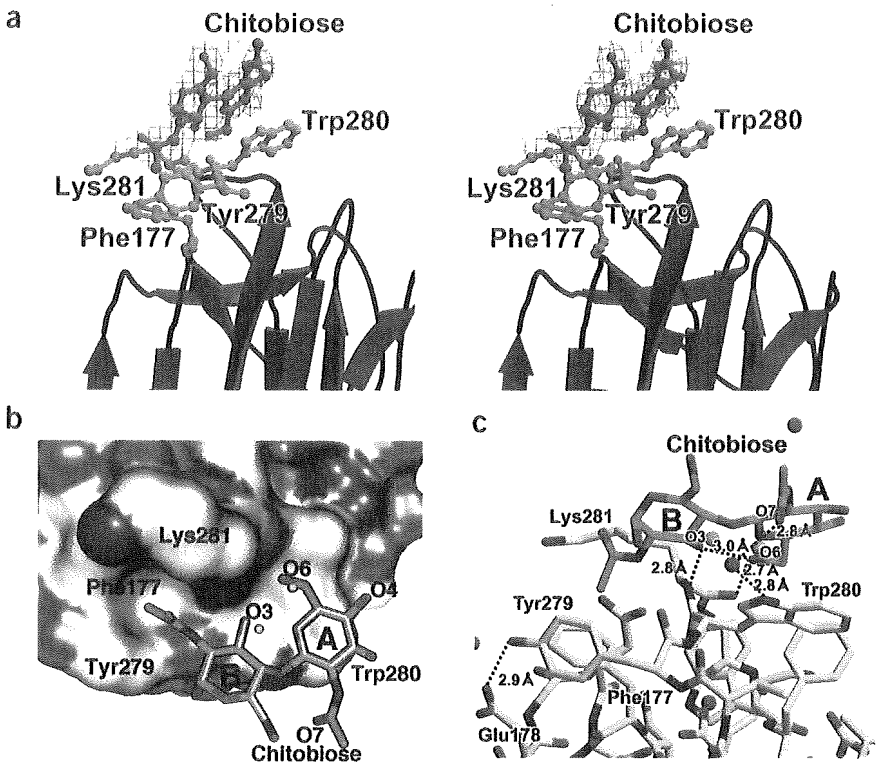

Figure 2 Structure of SBD in complex with chitobiose. (**a**) Stereo view of the difference-density map ($F_o - F_c$ with phase from the Fbs1 model) of binding chitobiose, contoured at 2.1 σ, modeled into the electron density. β-strands belonging to S1 and S2 are blue and red, respectively. Loops are black. The bound chitobiose is orange, and the residues involved in the substrate binding (FYWK, see **Fig. 1c**) are green. (**b**) Molecular surface representation of the chitobiose-binding region. The bound chitobiose is shown in ball-and-stick representation. Two GlcNAc residues are represented by A and B. Cyan spheres are two water molecules of wild type SBD that are fixed on the molecular surface through hydrogen bonds with the backbone N and O of Lys281, respectively. These water molecules are replaced by O3 and O6 of the chitobiose upon formation of the SBD–chitobiose complex. (**c**) Stick representation of the amino acids involved in binding. Hydrogen bonds are dashed lines. Oxygen and nitrogen are red and blue, respectively. Symbols of two water molecules are as in **b**.

To verify that the crystal structure accurately represents the complex formed in solution, we introduced point mutations into the residues in the pocket, and examined the *in vitro* activities in binding the ribonuclease B (RNase B) carrying a high-mannose oligosaccharide (**Fig. 3a**). Indeed, F177A, Y279A and W280A mutations reduced binding to the RNase B, whereas the K281A mutation had no effect on the binding (**Fig. 3a**, left panel). We next tested the *in vivo* activities of these mutants in binding the precursor of integrin β1, one of the *in vivo* Fbs1 targets[7] that contains high-mannose oligosaccharides. Consistent with the *in vitro* results, F177A, Y279A and W280A, but not K281A, failed to bind integrin β1 (**Fig. 3a**, right panel). These results suggest that Phe177, Tyr279 and Trp280, located in the hydrophobic pocket at the edge of the β-sandwich, are important for interaction with chitobiose in the high-mannose oligosaccharides. In contrast, although comparison of the structure of the SBD alone and that of the SBD–chitobiose complex indicated that the side chain of Lys281 underwent a conformational change upon ligand binding, the *in vivo* and *in vitro* binding studies suggested that this conformational change was not essential for the recognition of oligosaccharides. Moreover, we examined the impact of these mutants on the ubiquitinating activities of the SCF onto GlcNAc-terminated fetuin (GTF) *in vitro* (**Fig. 3b**). SCF (Fbs1-W280A), which could not bind to N-glycans, failed to ubiquitinate GTF, whereas the ubiquitinating activities of the K281A mutant were retained. Taken together, these results indicate that the hydrophobic interactions between GlcNAc(A) residue and Trp280, and of GlcNAc(B) residue with the small hydrophobic pocket, are required for substrate recognition. In addition, the hydrogen bonds between the chitobiose and Fbs1 atoms (Nε1 of Trp280 and the carbonyl oxygen atom of Lys281) are involved in selective binding to chitobiose.

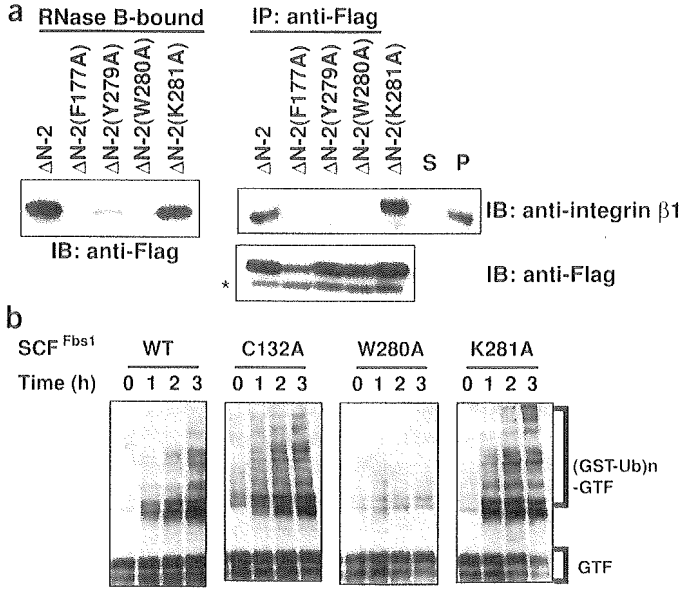

Figure 3 Residues required for interaction of Fbs1 and glycoproteins with high-mannose oligosaccharides. (**a**) Neuro2a cells were transfected with Flag-tagged Fbs1 (ΔN-2) and its listed derivatives. In pull-down assay (RNase B-bound), each ΔN-2–expressing WCE was incubated with RNase B–immobilized beads; bound proteins were eluted by 0.1 M of chitobiose and then analyzed by immunoblotting with an antibody to Flag (anti-Flag). In immunoprecipitation with anti-Flag (IP: anti-Flag), the Fbs1-binding proteins in the immune complex were analyzed by immunoblotting using the anti-Flag or anti-integrin β1 antibody. Asterisks indicate the light chain of IgG. (**b**) *In vitro* ubiquitination of GTF by the SCF^{Fbs1} E3-ligase system. The high-molecular-mass ubiquitinated GTF [(GST-Ub)n-GTF] was detected by immunoblotting with an antibody to fetuin.

NMR analyses of the SBD-sugar interactions

We have previously reported that Fbs1 shows higher affinity to $Man_{3-9}GlcNAc_2$ glycans than to chitobiose, and the number of mannose residues did not influence the affinity[8]. We conducted NMR spectroscopic analysis to determine the contribution of the outer